MICRO-PATTERN GASEOUS DETECTORS

Fabio Sauli
(CERN, Geneva, Switzerland)

Archana Sharma
(GSI, Darmstadt, Germany)

ABSTRACT

Introduced ten years ago, micro-strip gas chambers have substantially better performance than classic multi-wire detectors: excellent localization, high rate capability, good granularity make them very attractive for tracking at high luminosity colliders, as well as for other applications. A substantial and successful development effort has been undertaken to improve the technology, with the development of supports preventing charge accumulations. Some problems persist however, namely the slow degradation under sustained irradiation (aging) and the serious damages that can be produced by accidental discharges. New types of detectors, recently introduced, aim at improving on these points; micro-dot, micromegas, gas electron multiplier are promising examples. They have in general higher reliability, and can be produced at lower costs.

CONTENTS

PERFORMANCE AND LIMITATIONS OF MULTI-WIRE DETECTORS

Introduced in 1968 by Georges Charpak, at the European Laboratory for Nuclear Physics (CERN) in Geneva (1), the multiwire proportional chamber (MWPC) revolutionized instrumentation used in experimental particle physics. Exploiting avalanche multiplication around thin anode wires, the MWPC permits fast detection and localization of small amounts of charge released in a gas by ionizing radiation. Numerous and variously named generations of multiwire gaseous devices have been developed from the original progenitor: drift, time projection, time expansion, ring-imaging chambers are some examples. For an exhaustive coverage of the subject, see Refs. (2-7). Gradually replacing slower tools, multiwire devices of various designs have been, and are still today, major components in detectors for particle physics. Their use has successfully spread in other applied research fields: astrophysics, industrial and medical diagnostics, biology (8, 9). In recognition to his invention, Charpak was awarded the 1992 Nobel Prize for Physics.

Confronted with the increasingly tough demands of particle physics experiments, MWPC have been continuously improved over the years to provide better performances. Several limits however have been met, namely in rate capability and granularity. Placing and holding the thin anode wires at distances closer than a few mm turned out to be hard. Moreover, the electrostatic repulsion between thin anodes leads to instability above a critical wire length, below ten cm for one-mm spacing. A more fundamental hindrance is the copious production of positive ions in the avalanches, only slowly collected by the electrodes, and generating a distributed positive space charge that modifies the electric field. As a consequence, the

proportional gain of the detectors drops quickly at a radiation flux above ~10^4 s^{-1} mm^{-2}. Attempts to resolve the mechanical limitations gluing the wires on insulating supports were proposed long ago (10), followed over the years by several, often undocumented efforts; the micro-gap wire chamber is a recent variation on the theme (11). Difficult to implement, and with non-uniformity of operation introduced by the contact with insulators and glues, these devices had only limited success.

In 1988, Anton Oed, at the Institut Laue-Langevin (ILL) introduced a novel concept in Grenoble: the micro-strip gas chamber (MSGC) (12). Consisting of a set of tiny metal strips engraved on a thin insulating support, and alternatively connected as anodes and cathodes, the MSGC relies for its operation on the same processes of avalanche multiplication as the multi-wire devices. The photolithography technology used for manufacturing, however, permits to reduce the electrode spacing by at least an order of magnitude, correspondingly improving the multi-hit capability. Moreover, the fast collection of most positive ions by the nearby cathode strips reduces space charge build-up, and provides a largely increased rate capability. Introduced coincidentally with the first projects of high luminosity colliders, MSGCs filled a gap in the available detector technologies, between solid state strip detectors, having excellent performances but high costs, and the cheap but rate-limited traditional gas devices. Intensively developed by many research groups, MSGCs have been adopted as components in high rate tracking setups for major experiments. For HERA-B at DESY, several hundred large MSGC plates, 30 cm on the side, have been built; the CMS detector, in construction for the LHC collider at CERN, will deploy around 16,000 modules, in arrays covering a sensitive volume of tens of cubic meters.

Despite their impressive performance, detailed studies on high rate, long-term behavior have shown some possible weaknesses of the MSGC technology. Polymerization processes, occurring in the gas under sustained avalanche conditions, result in the deposition of thin insulating layers on the electrodes, and affect the performances. Discharges provoked by imperfections in the artwork, or triggered by abnormally large energy losses, can permanently damage the thin electrodes. In a wide effort to find more performing and reliable devices, alternative detector concepts have emerged in the recent years. Between them, the "Compteur à Trous", or CAT (13) makes use of the avalanche multiplication in narrow holes. Micromegas (14) exploits high gain properties of narrow gap parallel plate multiplication. The micro-dot (15), a matrix of individual circular counters laid on a substrate, probably represents the ultimate gaseous pixel detector. Last born, the gas electron multiplier, GEM (16), has the unique feature of permitting the sharing of the overall gain necessary for detection in a cascade of elements, each operated below the critical voltage for discharges, with a large improvement in reliability.

Starting from the original work on micro-strip chambers, this paper describes developments, major achievements and unsolved problems of the technology. It continues with a summary of recent developments of several new devices, collectively named micro-pattern gas detectors, and attempts a critical discussion of their performances and limitations. In view of the large number of papers, more than three hundred published on the subject in the recent years, the authors had to make an excruciating selection on the material to be included. They refer the reader to the extensive list of references for more information, and apologize for omissions. A good coverage of the basic physical phenomena underlying the detector action in gaseous counters can be found in the quoted literature, as well as in numerous textbooks (17-20).

MICRO-STRIP GAS CHAMBERS

Basic structure and operation

The micro-strip gas chamber consists of a set of thin parallel metal strips, laid on an insulating support, and alternately connected as anodes and cathodes; Figure 1 shows a close view of the anode ends in one of the first plates developed at ILL (12). The rear side of the support plate can also have a field-defining electrode, the back-plane, full or segmented to perform two-dimensional localization. Using accurate but simple photo-lithography technologies, a distance between strips, or pitch, of one hundred microns can be obtained, with an order of magnitude improvement in granularity over wire chambers. Mounted within a gas vessel, with an upper drift electrode delimiting the sensitive gas volume, the MSGC permits to detect ionization released by radiation. With appropriate potentials applied to the electrodes, negative with respect to the anode on both drift electrode and cathodes, electrons released in the drift space move towards the strips, start to multiply approaching the high field region close to the anodes, and generate detectable signals. For convenience, the strips destined to be read-out are kept at ground potential, while the other are powered in groups through high value protection resistors. Figure 2 shows the electric field equi-potentials and field lines in the vicinity of the strips, computed with anodes and back-plane at equal potentials (other configurations will be discussed later). All field lines from the drift volume terminate on the anodes, providing full electron collection efficiency. Due to the broad spread of the avalanche, however, a large fraction of the positive ions generated at the anode spills over the field lines connecting to cathodes, and is quickly collected. This largely reduces space charge accumulation, and provides a much higher intrinsic rate capability as compared to classic devices. Moreover, a large fraction of the signal is induced by the rapidly moving ions, resulting in a fast rise time.

At the occurrence of an avalanche, the fast electron collection and the retrograde motion of ions generate negative signals on the anodes. Signals of opposite polarity are induced on the neighboring cathodes and on the back-plane electrode. Due to mutual capacitance, a fraction of the signal induced on one set of strips is injected into the other, with amplitude and extension that depend on the grouping scheme, giving the typical charge profile shown in Figure 3.

High gains, very good proportionality and resolution have been obtained in a wide range of X-ray energies, essential features for astrophysics applications (21). Together with the good position and multi-track resolutions, these characteristics made the MSGC very attractive for detection of high rate, high multiplicity events. From the very beginning, however, various operating instabilities were observed, particularly at high rates: time-dependent gain shifts, attributed to substrate polarization and charging up, permanent deterioration (aging) during sustained irradiation, and a tendency to discharge (22, 23). The physical parameters used to manufacture and operate the detectors (substrate material, metal of the strips, type and purity of the gas mixture) appeared to play dominant roles in determining the medium- and long-term stability. A big effort was undertaken to better understand the MSGC operation, to improve their performance and lifetime, as well as to reduce manufacturing costs, an essential goal in view of intensive use in large systems. At the peak of its activity, a collaboration for the development of MSGCs included more than 40 laboratories worldwide. For general overviews the reader is referred to review papers (24-26) and to the proceedings of two dedicated workshops (27, 28).

Electric field configurations

The electric field structure in MSGCs has been studied with a variety of tools, from simple analytical approximations to sophisticated models taking into account also dynamic charging up processes (29, 30). Computer codes can be used to map the electric field in complex multi-electrode structures, and to evaluate drift, diffusion and multiplication processes (31, 32). The field is constant over most of the sensitive volume, controlled by the drift voltage V_D. It increases towards higher values in the proximity of the strips, where a negative potential V_C applied to the cathodes, anodes being grounded creates the multiplying field. With the anode strips narrower than the cathodes, the field strength can be made sufficiently high for electron multiplication, at the same time maintaining the field at the surface of the cathode below dangerous values. The field in the drift region is reduced on application of the cathode potential, and is approximately given by $E_D = (V_C - V_D)/g$.

Computed for the conditions of Figure 2, the plot in Figs. 4 (solid lines) provide the field strength on a line just above the plate surface, originating at the anode's center. The field is uniform over most of the strips' width; the large increase at the ends is responsible for a local increase of gain, and for an enhancement of the field emission probability at the cathode edges.

For insulating supports, the presence and value of the potential applied to the back electrode, V_B, plays an important role in the operation. A back plane potential close to V_C enhances the multiplying field, permitting to obtain larger gains, but results in a number of field lines entering the dielectric, as seen in Figure 5. A fraction of the ions produced in the avalanches reach the support and stick to the surface, dynamically changing the field, until a new equilibrium is reached at a reduced value of gain. As the equilibrium depends on production and neutralization rates, in general varying from place to place, the operation is unstable. Decreasing V_B towards the potential of the anodes, an optimum condition can be found where no field lines enter the dielectric; this was the case shown in Figure 2. Due however to collisional diffusion of ions during their drift, surface charging up and instabilities can still occur, albeit at higher rates.

Use of supports with reduced resistivity permits to neutralize the surface charge, and extends considerably the rate capability of the MSGC. For thick, bulk conducting supports, the structure of the electric field is identical to the case of an insulator. Such is not the case with a thin conduction layer, where as a result of surface currents the field between anodes and cathodes is made more uniform, increasing along the gap, and decreasing close to each electrode, as shown by the dashed curves in Figure 4. This modification of the field entails the need of increasing the voltages to obtain similar gains. A conducting layer acts also as an effective screen for the voltage applied on the back plane, which can be eliminated altogether, unless needed for signals pick-up.

Manufacturing technologies and choice of the substrate

For proper operation of detectors, quality of the support and of the metal used for strips have to satisfy strict mechanical and electrical requirements. Adherence of the strips to the substrate must be excellent, to protect against accidental release of conducting fragments (the worst fear for gaseous counters). The surface of the metal itself must be smooth, without field-enhancing roughs, and edges of the strips well defined, and possibly not too sharp. No unique choice satisfies all requirements, each

having its own advantages and drawbacks. Of all metals used, chromium is one of the sturdiest, and the only one that can withstand mild discharges without damages, thanks to its high melting point. However, mechanical stress building-up during deposition can induce micro-cracks and deformations above a thickness of 2-3000 Å. For thin anodes, the ensuing resistivity of several $k\Omega$ cm^{-1} generates a position-dependent attenuation in high rate applications that require the use of low impedance amplifiers. With its considerably lower resistivity, gold is a better choice; the technology for manufacturing gold strips is however more difficult and expensive. Moreover, because of its low melting point, sparking can induce serious damages to the strips. Aluminum offers a good compromise between mechanical and electrical characteristics, and has been adopted for the first, medium size experimental set-ups. Under irradiation, however, aluminum MSGCs have been found to suffer a considerable degradation of performances with time, even after modest amounts of collected charge.

Depending on the metal, different methods are used for its deposition on the substrate, often in association: vacuum evaporation, sputtering, electro-chemical or galvanic growth. Except for chromium, bonding extremely well to glass, most metals are not applied directly, but over a previously evaporated, thin adhesion layer, usually nickel and/or chromium. Platinum is often used as migration barrier before gold and silver deposition, to prevent diffusion into the substrate.

Several techniques have been used for manufacturing MSGC plates. In all cases, the final module is the direct or inverted copy of a master pattern, realized with high precision by direct, computer-controlled, laser or electron beam ablation. Using conventional, single-mask photolithography two methods, with a number of variants, have been used industrially to produce the plates:

- Direct photolithography (Figure 6a): the metal-coated substrate is covered with a thin layer of photosensitive resin. A positive mask is overlaid, and exposure to ultra-violet light modifies the open areas, that are chemically removed after curing. Immersion in a solvent (wet etching), or ablation with reactive plasma (dry etching) eliminate the metal from the unprotected areas; the residual resin is then removed, and the plate thoroughly cleaned. The technology has been successfully used with chromium and aluminum, and permits to manufacture large area plates (up to 30x30 cm^2) at acceptable costs.

- Lift-off (Figure 6b): the support is prepared with a thin metal adhesion layer, and coated with the photosensitive resin. Exposure to UV light through a negative mask, curing, and removal of the exposed areas leaves a protection over the regions to be freed. The desired metal is uniformly grown by one of the processes mentioned above. Immersion in a solvent removes the polymer, and the overlaying metal "peels off"; a further short etching step then eliminates the adhesion layer in the open regions. Intrinsically more delicate and expensive to implement, the lift-off technology permits to engrave patterns in any metal, and even to make composite layers of different metals. It has been mainly used to manufacture MSGCs with gold and aluminum strips.

Other, more sophisticated methods using micro-electronics technologies with multiple masks permit the realization of more complex patterns, including insulating layers between electrodes (33). More expensive, and size-limited by the current silicon wafer technology, they have been used so far mostly for prototype works.

Excellent surface quality, good metal adhesion and high dielectric rigidity are particularly important parameters for obtaining reproducible and stable operation of the detectors. Some applications also demand a light and thin substrate to decrease multiple scattering and photon conversions. The requirements are met by

commercially available glasses, such as the boro-silicate DESAG D-263 and the alkali-free AF-45[1]. Other rigid supports have been used: quartz, silicon, ceramics, sapphire, as well as flexible thin-foil polymers. Most insulators with good surface quality have very high resistivity, above 10^{16} Ω cm; it was recognized soon that this could generate instabilities due to local charge redistribution. A fine tuning of the back-plane potential, in order to minimize the field lines entering the dielectric, and a high value of the drift field permit to obtain a reasonably stable operation at moderate rates. In most cases, however, a substantial increase of resistivity at power on, accompanied by a decrease of gain (Figure 7), and a rate-depended gain shift (Figure 8) have been observed (22, 23, 34-36). The effects are attributed to a dynamic modification of the electric field following the application of voltage, and due to substrate polarization, internal rearrangements of the charge carriers, and surface charging up.

Thermal treatments, voluntary or part of the manufacturing process, may alter the surface conductivity, and can lead to inconsistent results; this appears to be particularly the case when using wet etching manufacturing (23). Also, since alkali ions are very mobile in glass at high temperature, internal redistribution may occur if the plates are heated up for cleaning. Using silver as metal for the electrodes, an enhancement of conductivity, imputed to the diffusion of ions into the glass, has been found to improve the stability of operation (37). A visible depletion of the metal from the strips has however been observed, making this solution unsuitable for long-term operation.

Use of a substrate with lower resistivity and dominant electron conduction eliminates most of the above mentioned problems. Somewhat improperly named semi-conducting, specialty glasses with resistivity in the range 10^9-10^{12} Ω cm have been developed for various applications; they are often called Pestov glasses, from the major developer (38); some are commercially available (S-8900[2]). Using MSGCs manufactured on semi-conducting glass, excellent high rate performance and long-term stability have been demonstrated (23, 39-44). Examples are shown in Figure 9 (40). For a glass with resistivity of 10^9 Ω cm, no gain drop is observed up to and above an X-ray flux of one MHz mm^{-2}. Since the leakage current increases with the conductivity, and is an intrinsic source of noise, there is obviously no advantage in reducing the resistivity below the value imposed by the rate requirement.

However promising, bulk conducting glass is expensive and fragile to handle, particularly in thin layers. Similar characteristics can be obtained reducing only the surface resistivity to equivalent values between 10^{14} and 10^{15} Ω/square. Several methods of conditioning insulating supports have been explored to obtain values in this range. Early tests with phosphor and boron implantation in quartz and silicon oxide were reported in Refs. (21, 45, 46). Some doubts exist however on the long-term stability of the implants, most ions being rather mobile in amorphous glass.

Deposition over the insulating support of an electron-conducting layer is an intrinsically simpler technique to control surface resistivity. Thin layers of lead silicate with the desired values of resistivity have been deposited by reactive magnetron sputtering (47, 48), and tested successfully on MSGC plates (49). Using a semi-conducting glass target, a conductive layer can been directly sputtered over thin substrates (50, 51). Good uniformity over large areas can be obtained by chemical vapor deposition of diamond-like carbon (DLC) layers, chemically treated to provide the required resistivity[3]. Detectors made with this technology have been

---

[1] Deutsche Spetialglas AG, Grünenplan (D)
[2] Schott Glass Technologies, Dureya PA (USA)
[3] SURMET Co, Burlington MA (USA)

extensively tested, and appear to be uniform and stable in a wide range of resistivity (52-55). An example of gain measured as a function of rate, for MSGC plates built on a diamond-like coated support is shown in Figure 10. Using a similar deposition process, several hundred large area (30x30 cm^2) thin glass plates have been coated to serve as substrate for the large MSGCs built for the HERA-B experiment at DESY (56). It should be noted that, stable at room temperature, most semi-conducting layers evolve into higher resistivity when raised at temperatures above 100°-150°C, particularly in presence of nitrogen (54). This prohibits the use of post-processing requiring high temperatures, such as baking and polyimide passivation.

Other technologies for surface resistivity reduction have been studied, such as ion-beam sputtering of amorphous hydrogenated silicon, carbon and silicon carbide (57-59). Encouraging results have been obtained with thin layers of aluminum nitride (60).

In all described methods of surface conditioning, the insulator is coated before metallization and patterning. This can create problems because of poor adherence of the metal, and of local imperfections due to uneven deposition or dust inclusions. Covering a completed MSGC structure with a thin resistive layer (over-coating) is intrinsically safer. Promising results have been obtained using thin metallic layers, such as nickel (61), copper and germanium (62), lead oxide and doped polymers (49). A systematic degradation of structures subjected to long-term irradiation has been however reported, discouraging the use of the over-coating technology for high rate applications (63).

Various attempts have also been made to use thin polymeric foils as supports. Polarization and charging-up can be avoided choosing a material with moderate resistivity, or by ion implantation (64-68). In general, however, because of modest surface quality and poor metal adherence, added to high manufacturing costs, the results were only moderately successful.

Optimization of design and operation

A particular effort has been undertaken to optimize the design of the detectors for high rate tracking of minimum ionizing particles; with a required operating gain of a few thousand, a reachable gain up to 10^4 is considered necessary to ensure a safe operation. As intuitive, the best performances can be obtained with thin anodes; practical considerations restrict the minimum values between 5 and 10 μm. Decreasing the open gap, making the cathodes wider, helps reducing the voltage required for a given gain. At very narrow gaps, however, and presumably due to imperfections in the artwork and support, the appearance of discharges limit the maximum gain, as shown in Figure 11 (69). An optimum is reached for a width around 90 μm, an aspect ratio metal to insulator of ~50%. A detailed study of the single electron noise spectra close to the maximum confirms the hypothesis that discharges can be triggered by avalanches initiated by electrons released at the cathode edge, by ion bombardment and field effect (69).

Detection of fast particles in few mm thick layers requires the use of gases with favorable ionization statistics. Best results have been obtained using dimethyl-ether (DME); at one bar, minimum ionizing particles have in DME 55 ionizing encounters per cm, as against 25 in argon and 15 in neon. To avoid having to reach excessive voltages, DME is used admixed with noble gases (70-73); examples are given in Figure 12. Other gases tested include mixtures with CF_4 (74), having the advantage of a faster drift velocity, and reported to prevent or even cure aging.

Assembly of detector modules

Several schemes have been used to assemble MSGC detectors. For laboratory measurements, a vessel with high voltage and signal feed-through is convenient for testing individual plates. A similar scheme has been adopted in some experimental set-ups, with several arrays of plates mounted within a large gas box (75). Lighter and cheaper assemblies have been developed, in view of the construction of large modular arrays. As shown schematically in Figure 13, a module is manufactured with a thin rectangular insulating frame glued directly on the rigid engraved plate; a second thin glass plate, conductive on the inner side, is glued to the frame and constitutes the drift electrode (76). Holes in the frame allow the flow of the filling gas. Other groups have developed similar schemes.

Micro-strip plates with non-parallel geometry have been developed for the specific needs of forward trackers in particle physics; in the so-called keystone or wedge-shaped geometry, strips fan out from a minimum to match the angular divergence of tracks. By proper design of the strip width and spacing, a rather uniform gain can be obtained along the strips, despite the varying pitch (77, 78)). Several plates can be assembled edge to edge inside a common box, with the readout electronics inside or outside the gas vessel. The picture in Figure 14 shows a prototype with eight wedge-shaped MSGC plates, mounted in contact in a semi-circular module (the so-called closed banana) (79), developed for the CMS Forward MSGC detector. The detailed geometry of the joints (or cracks) has been thoroughly studied to minimize losses (80, 81).

In most MSGC designs, anode and cathode strips are, for convenience, connected on opposite sides. The electric field is strongly perturbed in the vicinity of the ends of the strips; the cathode end side is particularly affected, and, discharges can easily take place even at low voltages. Several studies have attempted to optimize the geometry of the strip ends, with rounded tips and/or an increase of the open gap, in order to reduce the field singularity (82, 83). In general however, and in order to reach the high voltage required for detection of small amounts of ionization, coating (passivating) the critical area with an insulator is a safer solution. The coating material has to possess excellent dielectric rigidity and low outgassing, and the curing method has to take into account the possible effect on the other components.

Detection and localization of charged particles

Prototypes of various designs have been extensively tested in the laboratory and in test beams to study their performances in the detection of minimum ionizing particles (78, 84-94). Small but complete systems have also been successfully used as high-precision trackers in physics experiments (75, 95-99). Developed for the requirements of silicon micro-strips, several highly integrated circuits have been adapted to MSGCs; they generally have fast shaping times, typically 30 to 60 ns (100). Because of the particular characteristics of induced signals, with the major contribution given by the motion of ions, this implies a considerable reduction of the detected charge (the so-called ballistic deficit). Detailed analysis of the signal shape in various load conditions, and of their effects on resolution has been made (101, 102). Some calculations include a detailed monte-carlo simulation of the ionization statistics and charge collection processes (103).

At high rates, and in order to reduce the probability of accidental overlap of signals (the so-called occupancy), the electron collection time has to be minimized. This is achieved using narrow detection gaps (two to three mm), a fast gas mixture

and high values of the drift field. Figure 15 gives an example of total charge collected, for minimum ionizing tracks perpendicular to a MSGC operating at gains of a few thousand; it has the characteristic Landau shape. The small peak at the left represents the noise. The signal over noise ratio, defined as the most probable value of the charge divided by the rms of the noise, is only around 15. While more favorable values can be obtained increasing the voltage, this can lead into a region of unsafe operation. Examples of efficiency plateaus for fast particles, perpendicular to the detector, and in a range of gas fillings are given in Figure 16 (87).

Position accuracy for perpendicular tracks better than 40 μm rms was demonstrated in early works (104), and confirmed since by many measurements. The cluster size, or mean number of anode strips with signals over threshold for each track, is around 1.5 for 200 μm pitch; in these conditions, two tracks 500 μm apart can be fully resolved (78). Because of the dispersions introduced by the primary ionization statistics, the accuracy worsens for tracks at increasing angles with the normal, as shown in Figure 17 (105). The cluster size widens correspondingly, and because of the sharing of charge between strips it is increasingly hard to obtain good detection efficiency.

Operation in strong magnetic fields is required in some experiments; a non-zero magnetic field component in the direction of the drift imparts a deflection to the electrons' swarm, the Lorentz angle, whose value depends on gas and fields, and affects the drift velocity. This can introduce a degradation of performance. DME-rich mixtures and high drift fields are favorable to diminish the distortions; at 4 Tesla, the Lorentz angle can be reduced to around 15°, and compensated, at least for a parallel tracks field, slightly rotating the detectors. This solution has been adopted for the CMS tracker, after systematic measurements with prototypes operating in strong magnetic fields (106, 107).

Two-dimensional readout

The fast collection of electrons, and the retrograde motion of ions induce signals on the anodes and all surrounding electrodes. As shown already in early works, the back-plane electrode can be segmented or stripped to provide an independent coordinate. The fraction of induced signal depends on the ratio between pitch and support thickness (108). Applying a more negative potential to the back plane, the signal increases, at the expense of a reduced rate capability (109). The two-dimensional neutron absorption image shown in Figure 18 has been obtained with the described device.

A way to increase the back-plane signal is to leave the cathodes floating (110). Removing the metal from most of the strip surface, leaving only the edges to define the field, permits to obtain large signals on the back plane (108); however, to avoid severe charging-up problems, this can be achieved only using supports with reduced resistivity. Using a bulk electron conducting glass, one can obtain a reasonably stable behavior, at least for moderate rates, even removing cathodes altogether in the so-called asymmetric or virtual cathode chamber (108, 111).

Using integrated circuits technologies, a double metal structure, separated by a very thin insulating layer, can be grown on the top of a thicker support. Two-dimensional devices of this design have been built, with a few microns thick ion implanted silicon oxide (112, 113) or a thicker polyimide film separating the two metallic coatings (114-116). With almost identical signal amplitudes on the anodes and back plane strips, an excellent correlation between the two coordinates has been demonstrated. An essential requirement for this design is that the thin insulator

holds the operating voltage between cathodes and back-plane without leakage or discharges. This turns out to be rather difficult with thin silicon oxide films; polyimide, that can be grown up to several tens of microns, is a better choice. Due to its intrinsic high cost and size limitations, the technology has not yet been exploited for large systems.

Long term performance: discharges and aging

Despite their promising performances, experience with MSGC has raised several doubts on the long-term behavior. Two major problems have been met, at various degree of relevance, depending on the applications: rare but often damaging discharges, and slow but continuous deterioration (aging) during sustained irradiation.

The appearance of discharges during operation is a permanent problem with all gas micro-pattern detectors, and has been extensively analyzed in studies exceeding the MSGCs framework (70, 117-122). The general conclusion is, that when the total charge in the avalanche exceeds a value between 10^7 and 10^8 electron-ion pairs (Raether's limit), an enhancement of the electric field in front and behind the primary avalanche induces the fast growth of a long, filament-like streamer. In the high fields and narrow gaps typical of micro-pattern devices, this leads to discharge, with damaging effects on the strips as seen in Figure 19. Depending on conditions, a discharge can injure the strip or, in the worst case, produce a local short circuit. Low melting point metals such as gold and aluminum are easily damaged, while others as chromium and tungsten are more resistant (123, 124). At the gains required for detection of minimum ionizing particles in thin gaps, typically above 2000, the accidental release of larger amounts of ionization easily brings the total charge above the limit. For reasons that are still not completely understood, a high rate of low ionizing power radiation produces a similar effect.

The behavior of detectors exposed to large ionization losses can be emulated in the laboratory with exposure to alpha particles, from an external source or internally emitted by ^{220}Rn injected in the gas flow and generated by a cartridge containing thorium oxide. A very fast increase of the discharge probability with the operating voltage is observed at gains above a few thousand, as shown in Fig, 20 (125). Detailed studies of the process, extended to other designs of detectors, suggest that all single-stage micro-pattern detectors suffer from the same basic limitation, overcome only if the multiplication process is shared between cascaded devices (120).

Various schemes have been used to try and limit the damages produced by a discharge. Reducing the available energy by connecting small groups of strips to the voltage with limiting resistors helps, but correspondingly increases the opposite polarity signal pickup. Alternatively, a series resistor, ~1 kΩ, added at the amplifier's input limits the energy flow, but affects the signal rise time (96). Coating of the cathode edges with a thin polyimide insulator, the so-called advanced passivation, has been claimed to prevent discharges up to very high gains (126), an observation not confirmed by other authors (119, 120).

Aging, the slow degradation of performance during sustained irradiation, is a problem encountered with most gaseous counters, and has been extensively studied experimentally (for a review see (127, 128)). The observed permanent damage of the plates has been imputed to the production of polymeric compounds in the avalanches, sticking to the electrodes or to the insulator, perturbing the counting action and inducing discharges. MSGCs have been found to be particularly prone to

aging, possibly because of the small effective area used for charge multiplication. Organic gases like hydrocarbons induce very fast aging, while others, such as dimethyl-ether and carbon tetrafluoride, allow more extended lifetimes. A careful selection of the operating gas and of the materials used in manufacturing is mandatory to guarantee survival of the devices in a high radiation environment (129, 130). Figure 21 shows an example of the dramatic difference in aging rate obtained for identical plates using a conventional detector assembly with fiberglass and epoxy, and a cleaner containment vessel (131). Equal being other conditions, use of a low resistivity support permits higher levels of exposure without gain drops (40, 49, 132), possibly because of a reduced effect on the field of thin deposits. The nature of the metal used for the strips also appears to play an important role (71), gold being the best choice as shown in Figure 22 (133).

In optimal laboratory conditions, a long-term survival without degradation up to a collected charge above 100 mC cm^{-1} has been demonstrated by many groups (33, 35, 40, 67, 71). An example is provided in Figure 23, measured on a plate made with chromium strips on low resistivity glass, and using as construction materials those indicated by the quoted studies. Similar results have been obtained using MSGCs manufactured on thin electron-conducting layers (26, 33, 63).

Other developments and applications

Originally conceived for the detection of neutrons and X-rays, MSGCs owe most of their development to the demanding requirements of high rate tracking of charged particles. Many other applications have been developed, often with large improvements in performance over existing devices.

Continuing on the successful initial development, the group at the Institut Laue-Langevin has built and operated several position-sensitive neutron detectors; the largest system, the D-20 spectrometer, includes 50 medium-size MSGC plates operated in a ^{3}He-CF$_4$ gas mixture for optimal efficiency and performance. A smaller system, similar in conception, has been used to study single crystal neutron diffraction (134).

In the detection of soft and intermediate energy X-rays, the good energy and position resolution have been exploited for astrophysics (135). The high rate capability, particularly if coupled to digital read-out electronics, permits the fast realization of absorption radiographs (136). The high rate capability is also exploited in detectors for synchrotron radiation facilities (137). With gadolinium converter foils as drift electrodes, MSGC plates have been used for the imaging of thermal neutrons (138, 139).

The operation at low pressures has been extensively studied; a two-stage gain process, an initial parallel plate multiplication followed by the normal MSGC, permits the large gains needed for single electron detection (140). With the addition of an internal photo-sensitive electrode, such as evaporated CsI, the device becomes a very effective localizing detector for UV-light (141). Secondary emission from low-density layers of CsI or diamond-like carbon has been used for the detection of charged particles in devices capable of sub-nanosecond timing and with angle-independent localization property (142).

MSGCs with back-plane padded read-out schemes have been considered for the construction of improved time projection chambers, capable of better multi-track resolutions as compared to the classic design. Other advantages are the possibility of using short and non-parallel anodes, a higher rate capability, and a reduction of ion

feedback (143, 144).

High pressure operation has been investigated in view of the use as detectors for hard X-rays in medical diagnostics; despite the need to use increasingly high operating voltages, gains sufficient for detection could be reached in xenon mixtures (39, 145).

The scintillation properties of MSGCs have also been studied by various authors (146-148). Electron multiplication has been demonstrated using a MSGC in liquid xenon, a potentially far reaching development (149).

ALTERNATIVE MICRO-ANODE STRUCTURES

Micro-gap and small gap chambers

As discussed previously, a way to obtain two-dimensional projective readout in MSGCs is to reduce the thickness of the insulator separating anodes from back-plane. This can be achieved, with micro-electronics technologies, with the deposition of a few microns thick insulating film between metallic layers. The possibility of patterning electrodes and the insulating layer has led to the development of the micro-gap chamber (MGC) (150, 151), a structure in which the back-plane is used as a cathode, with thin anodes sitting on insulating strips, see Figure 24. The very small gap between anodes and cathodes permits to reach very high values of field, with a consequent faster signal rise time and shorter ion collection, a distinctive advantage of the structure. Bi-dimensional read-out is obtained patterning the cathode plane, with perpendicular strips or pads interconnected in a ladder-like structure for small-angle stereo readout.

Large gains, above 10^4, have been obtained with a MGC; mixtures of neon and dimethyl-ether seem to be particularly advantageous. Fast time response, good localization accuracy and high rate capability have been demonstrated (152, 153).

A high dielectric rigidity of the insulator between anode strips and cathodes is capital for operation. In the early devices a few μm thick silicon oxide insulating layer was used, applied by chemical vapor deposition. Further experience has shown however the non negligible probability of local defects (punch-through), hindering the realization of larger area detectors (154). In later MGC models, a thicker polyimide coating, several tens of μm thick, has been used successfully to ensure a better rigidity (155, 156). Thin polyimide strips have also been used to passivate the potentially dangerous high-field regions at the separations between cathode strips.

Operating properties of MGCs manufactured with different metals and in a range of geometrical parameters have been studied by several authors (50, 124, 157), as well as the resistance of the devices to local discharges (123). In view of medical applications, the operation in Xe and Kr at pressures up to six bars has also been investigated (158, 159). Several variants of the basic micro-gap structures have been studied, in view of improving their performances and reliability, in particular for what concerns the onset of discharges (156). Two recent developments, named small gap chambers, are shown schematically in Figure 25; the structures have been successfully tested in the laboratory and beam conditions (160, 161).

Micro-dot chamber

Manufactured with metal-oxide semiconductor technology, the micro-dot chamber (15, 154, 162) consists of a dense pattern of individual proportional counters made up with anode dots surrounded by annular cathodes; field-defining rings can

be added to improve the operation, as shown in Figure 26. The structure is built atop a thin oxide layer grown on a silicon substrate. To avoid charging up, the oxide can be ion implanted, or the completed device coated with a semi-conducting layer of boron-doped amorphous silicon carbide (163). For convenience of read-out the individual dots can be interconnected by a metal layer buried under the oxide. The role of the guard rings is to reduce field distortions induced in the multiplying cell by the interconnections; it effectively helps also to prevent the onset of discharges. Small size micro-dot devices have been tested in a variety of conditions and gas fillings; Figure 27 gives an example of the large gains that can be attained in argon-DME mixtures. Thanks to its fast response and exploiting the pixel structure, the micro-dot is ideally suited for applications requiring the simultaneous detection of multiple hits, such as Cherenkov Ring Imaging. Attempts to detect single photoelectrons have been however only partly successful, despite the large gains, because of the high level of noise induced by the large capacitance of the cells (164). This can be overcome operating the detector at low pressures, where gains in excess of 10^7 can be reached exploiting an initial parallel plate pre-amplification (165). The micro-dot detector is the only device that could withstand high gains under alpha-particle irradiation in a recent systematic study of discharge properties in micro-pattern detectors (120).

NOVEL MICRO-PATTERN DETECTORS

Thin-gap parallel plate structures, micromegas

The successful development of multiwire and micro-strip structure has somewhat sidestepped the research on gas detectors exploiting the multiplication in uniform fields. Mechanically sturdier, parallel plate multipliers have also intrinsically better energy resolution and higher rate capability. However, experimental data and theoretical considerations support the observation that the maximum proportional gain in parallel plate chambers is limited by the total amount of charge in the avalanche, around 10^7-10^8; above this value, the so-called the Raether limit, transition to a streamer occurs followed by breakdown. This has been confirmed in a wide range of operating conditions, and multiplying gaps (166-168). The exponential dependence of gain on the gap has also discouraged the construction of large area devices.

It has been recently found, however, that in sub-mm gaps exceptionally large gains could be attained, reaching the upper limit in the range allowed by the Raether condition (14, 122). This has led to the introduction of the micro-mesh gaseous chamber (micromegas) (14), see Figure 28. The detector consists of a thin metal grid stretched at a very small distance, 50 to 100 μm, above a readout electrode. With a very high field applied across the gap, typically above 30 kV/cm, electrons released in the upper drift region are collected and multiplied. The mesh itself, a standard component in high-resolution TV screens and usually made in nickel, is commercially available in large sizes and in a wide range of geometry. Regularly spaced supports (insulating fibers or pillars) guarantee the uniformity of the gap, at the expense of a small localized loss of efficiency. Essentially an avalanche counter with a Frisch grid, micromegas exploits the saturating characteristics of the Townsend coefficient at very high field to achieve a reduced dependence of gain on the gap variations, thus improving the uniformity and stability of response over large area. The main properties of parallel plate counters, namely rate capability and energy resolution, are maintained. Thanks to the small gap and high field, positive

13

ions move very quickly, and are mostly collected by the cathode mesh; this prevents space charge accumulation, and induces very fast signals with only a small ion tail, 50 to 100 ns wide. Operation at very high particle fluxes has been demonstrated: Figure 29 shows a measurement of current as a function of voltage, measured at increasing rates of a 20 MeV proton beam. The curves are parallel in a wide range of ionization density, demonstrating the absence of space charge distortions; the maximum gain however depends on the amount of charge. This is seen also in Figure 30, providing the maximum gain attained with the detector, as a function of the X-ray flux; at 10^5 Hz mm^{-2}, it exceeds 10^4 (169).

Efficiency and localization properties of the detector have been studied with several exposures to particle beams (170). Reasonable efficiency plateaus have been obtained for minimum ionizing particles, perpendicular to the chamber. Probably because of the poorly quenched gas mixtures used for the tests, that consent operation at moderate voltages, the lateral extension of the avalanche, or cluster size, was rather large (around one mm). Further studies with, better quenched gas mixtures and using fast readout electronics have achieved a substantial reduction of the cluster size, at the expense of a somewhat reduced efficiency plateau length (171).

Recent studies have demonstrated that micromegas, similarly to all single-step micro-pattern detectors, suffers from the basic limitation in gain, around a few thousand, when exposed to heavily ionizing tracks (120).

Trenches and holes, CAT and micro-CAT

The gain of a parallel plate counter depends exponentially on the gap thickness, making it hard to obtain a uniform response over large areas; the problem is exacerbated by the strong attraction between electrodes. Several ways have been proposed to circumvent the problem with the insertion of an insulating interface between the electrodes. An early example is the micro-trench gas counter, consisting in a sequence of wide anode strips buried within insulating channels with cathodes on the top (172). Charge amplification within narrow holes in a composite metal-insulator stack has been observed also with the high density drift chamber, a device designed for the conversion and detection of hard X-rays (173).

In the so-called "compteur à trous", or CAT, holes drilled through a metal-insulator sandwich are used to concentrate the field lines converging from a drift volume into a region of high field, where charge multiplication occurs, see Figure 31 (13). Even with relatively large holes, the good collection and focusing properties of the field result in rather good energy resolution at proportional gains up to 10^4 (Figure 32). The detected signal has, as expected, a fast electron and a slower ion component; the time length of the ion tail depends from the gap (several µs for one mm), and can be reduced to few hundred ns for narrower gaps. Several variations of the structure have been studied, with multiple holes and different shapes of the insulator plate, in order to minimize charging-up processes.

Similar devices, structurally equivalent to micromegas but named micro-CAT because of the use of cathodes with round holes, have been developed for the realization of two-dimensional X-ray imaging detectors (174). The effect on gain and energy resolution of the hole's geometry and gap thickness has been studied in a range of gas fillings and operating pressures, up to 6 bars. In view of medical applications, the authors have developed a cellular resistive read-out using a resistive anode foil padded with conducting lines, and forming a regular matrix of nodes, each connected to a charge-sensitive amplifier. With a detector operated at 3 bars, an accuracy of 200 µm fwhm for 8 keV X-rays has been demonstrated (175).

The gas electron multiplier

A way to obtain larger gains with parallel plate structures was devised some time ago by Charpak and Sauli, with the so-called multi-step avalanche chamber (176). Made with a succession of metal meshes, the detector multiplies ionization electrons injected from a drift region into a high field. A fraction in the avalanche is then transferred, through a lower field region, into a second element of multiplication, a parallel plate or a wire chamber. Despite the loss of charge in the transfer from high to moderate fields, effective pre-amplification factors of several hundred could be achieved. Followed by a standard MWPC, the device permitted the high gains needed for detection of single photoelectrons (177). Mechanically complex to implement, the multi-step chamber had only limited success, but demonstrated the great potential of subdividing the gain in several cascaded elements, separated by low-field gaps.

Introduced by Sauli in 1996, the gas electron multiplier (GEM) (16) consists of a thin, metal-clad polymer foil chemically perforated by a high density of holes, typically 100 per square mm (Figure 33). As shown in Figure 34, with a suitable choice of the voltages all electrons released by ionization in the overlaying gas layer are sucked into the holes, where charge multiplication occurs in the high field. Most of the electrons generated in the avalanches transfer then into the lower region; the GEM foil acts as a charge pre-amplifier, to a large extent preserving the original ionization pattern. The gain is a property of the GEM structure, and only mildly affected by the external fields, considerably relaxing the mechanical requirements. The GEM manufacturing method, developed at CERN, is a refinement of the double-side printed circuit technology. The metal-clad polymer (kapton) is engraved on both sides with the desired hole pattern; controlled immersion in a kapton-specific solvent opens the channels in the insulator.

The early measurements, and the first application of the technology have been made cascading the GEM amplifier with a standard MSGC (178-180). Figure 35 shows the gain characteristics obtained with such a two-stage detector; the rightmost curve corresponds to the characteristics of the MSGC alone, the others are obtained progressively increasing the voltage applied across the GEM foil. The cascaded device permits to reach much higher gains, or conversely, for a given required gain, to operate both MSGC and GEM well below their maximum safe voltage. Extensive tests under high flux and strongly ionizing particles irradiation have confirmed the large improvement of reliability of the two-step detector, adopted for the construction of the HERA-B tracker, originally based on large size MSGC plates only (119). Figure 36 shows the inventor holding a large GEM foil (25x27 cm^2 active), one of the several hundred made for the experiment[4].

The maximum gain that can be achieved with the GEM electrode depends on several factors: thickness of the polymeric support, diameter of the holes, gas mixture and applied voltages. In a systematic research effort, GEM devices have been improved to achieve proportional gains up to 10^4, suitable for direct detection of ionization on simple charge-collecting printed circuit board (PCB) electrodes. Optimum performance is obtained with 50 μm thick polymer foils, hole diameters 50 to 100 μm, and 100 to 200 μm pitch. Figure 37 show examples of gain measured with a single GEM in convenient, non-flammable mixtures of argon and carbon dioxide. Cascading two amplifying elements in a double GEM, gains well above 10^5 can be attained (Figure 38) (181-183). Systematic measurements with the structures show the

---

[4] Manufactured at CERN by the EST-MT group (A. Gandi, R. De Oliveira)

relation between detected current and applied fields. As an example, Figure 39 shows the signal current, detected on the PCB strips, increasing almost linearly with the transfer field; the balance is collected by the lower GEM electrode (183). The large increase of charge at the highest fields corresponds to the onset of charge multiplication in the transfer gap. The current due to positive ions divides between the top GEM and the drift electrodes; its constancy demonstrates that the true gain is unaffected by the value of the transfer field. Similar measurements provide the effect of the drift field in the collection efficiency, or transparency.

Single and the double GEM detectors with PCB readout have been extensively tested in the laboratory and in particle beams (184). Figure 40 shows the very comfortable efficiency plateau and the position resolution as a function of voltage obtained with a double GEM device.

It should be noted that in this mode of operation the signal detected on the strips is due entirely to the electrons collection, without slow ion tail, and is typically few tens of ns wide for a mm wide gap. The method can be extended to obtain a projective two-dimensional readout, using as pick-up electrodes double-level thin polymer foil with pads or strips interconnected in various patterns, see Figure 41 (185). Both read-out electrodes are kept at ground potential, a substantial advantage compared to other two-dimensional devices that require the use of high voltage decoupling capacitors. The method of manufacturing the pick-up electrodes is based on the one developed for the GEM meshes: two sets of parallel metal strips are engraved, using conventional printed circuit technology, on the two sides of a thin kapton sheet. After gluing the foil on a thin insulating support, the polymer in the interstices between the upper strips is removed with a solvent, opening the bottom layer to charge collection. Very good charge correlation between the two projections and position accuracy around 100 μm have been demonstrated. The signal induced on the lower GEM electrode can be used for triggering purposes, as shown in the figure. Figure 42 is a transmission radiography of the foot of a micro-mammal, realized with the described apparatus, and using an 8 keV X-ray generator as radiation source. The full size of the imaged area is 9x7 mm^2, and the quality of the image demonstrates the good resolution and low noise of the system. For particle tracking, the good charge correlation between the two projections represents a powerful tool for unambiguous reconstruction of multiple events.

Similarly to other micro-pattern devices, the GEM multipliers experience an increasing discharge rate under exposure to high radiation flux and highly ionizing tracks (120). Sharing the amplification process between two cascaded devices, however, results in a shift upward by at least an order of magnitude of the maximum sustainable gain. The dashed contour in Figure 38 provided, at the highest irradiation rate (5 10^5 Hz mm^{-2}), the upper boundary in the effective gain; a value well above 10^4 can be reached. Exposure to an internal alpha source produces a similar result. The trend to withstand larger amounts of charge when the second multiplier operates at lower potential supports the presumption of a voltage dependence of the discharge limit (120). The fundamental role of the low-field separation between multipliers, probably by suppressing photon- and ion-mediated feedback mechanisms, has been confirmed by reported failures of detectors directly combining two elements in contact.

The operation of GEM detectors has been studied in a wide range of conditions and gas fillings, for the detection of charged particles and X-rays (179, 186, 187) and of single photoelectrons, in view of possible applications in ring imaging counters and large area visible light imagers (188-190). A unique feature of the GEM structure is, with an appropriate choice of the fields and geometry, to considerably

suppress both photon and ion feedback from underlying structures into the sensitive volume. This has suggested using one or more GEM electrodes in devices aiming at the detection of single electrons emitted by an internal photo-cathode. Promising preliminary work in this direction has been already reported in detectors operated at low pressures (187, 189). The recent observation of high gains in pure argon with single and multiple GEM structures also supports the possibility of implementing bialkali semi-transparent photo-cathodes in a gas device (186, 188).

SUMMARY AND CONCLUSIONS

In the ten years since the introduction of the micro-strip chamber, an amazingly large number of studies aimed at a better understanding of the new detectors and improving their performance have been made. Confronted with the instability problems inherent in the use of insulating supports, research has concentrated on the development of controlled resistivity substrates; thin coating with diamond-like carbon and electron-conducting glass appear to be a reliable solution. Geometry, operating gases and metals used for the strips have also been the subject of extensive studies and optimization efforts. Successfully used in experimental set-ups requiring moderate proportional gains, MSGCs turned out to be prone to irreversible damages in harsher experimental conditions. Appearance of discharges on exposure to highly ionizing tracks has raised serious doubts on the reliability of large MSGC arrays of conventional design. Several ways have been proposed to circumvent the problem, from passivation of the cathode strips edges, to prevent the propagation of discharges, to fully innovative designs of the micro-pattern structure as in the micro-gap, micro-dot and small gap chambers. Potentially far reaching, these solutions require however sophisticated, multi-mask processing only available in the micro-electronics industry, as against the simple photo-lithographic methods used for manufacturing the standard MSGCs.

Recently, several new micro-pattern detectors concepts have been introduced, bringing big promises of increased reliability while preserving or even improving on performances over previous devices: among them, the "compteur à trous", micromegas, the gas electron multiplier. They share the common characteristics of lacking fragile thin anodes, gain being obtained by avalanche multiplication along an extended high field region. Manufactured with conventional, albeit innovative technologies, the new devices are also intrinsically cheaper and do not have the serious size limitations of micro-strip devices. One of them, the gas electron multiplier, has the unique feature to permit the pre-amplification and transfer of charge, essentially preserving the ionization pattern, into a second element of amplification. Sharing the required gain between two or more cascaded amplifiers, each operated at a voltage well below discharge, appears to be a sound way, if not the only, to solve the problems met with all single-stage micro-pattern detectors.

One hundred years after the invention of the proportional counter, and thirty after the multi-wire chamber, the development of high-performances micro-pattern devices is still today a challenging subject of research.

REFERENCES

1. Charpak G *et al.*, Nucl. Instrum. and Meth. 62 (1968) 262
2. Sauli F, CERN 77-09 (1977)
3. Sauli F, New developments in gaseous detectors, *in* Techniques and concepts of high-energy physics, T. Ferbel, Editor (Plenum 1983) 301-350
4. Charpak G & Sauli F, Ann. Rev. Nucl. Part. Sci. (1984) 285-349
5. Blum W & Rolandi G, Particle detection with Drift Chambers (Springer-Verlag, Berlin 1993)
6. Grupen C, Particle Detectors (University Press, Cambridge 1996)
7. Sauli F, Nucl. Instrum. and Meth. A419 (1998) 189
8. Sauli F, Nucl. Instrum. and Meth. A323 (1992) 1
9. Sauli F, Rad. Protection Dosimetry 61 (1995) 29
10. Neumann MJ & Nunamaker TA, IEEE Trans. Nucl. Sci. NS-17 (1970) 43
11. Christophel E & Dracos M, Nucl. Instrum. and Meth. A398 (1997) 195
12. Oed A, Nucl. Instrum. and Meth. A263 (1988) 351
13. Bartol F *et al.*, J. Phys. III France 6 (1996) 337
14. Giomataris I *et al.*, Nucl. Instrum. and Meth. A376 (1996) 29
15. Biagi SF & Jones TJ, Nucl. Instrum. and Meth. A361 (1995) 72
16. Sauli F, Nucl. Instrum. and Meth. A386 (1997) 531
17. Price W, Nuclear radiation detectors (McGraw-Hill, New York 1958)
18. Christophorou LG, Atomic and molecular radiation physics (Wiley, New York 1971)
19. Knoll G, Radiation detection and measurement (Wiley & Sons, New York 1989)
20. Delaney CFG & Finch EC, Particle Detectors: Physical Principles and Applications (Clarendon Press, Oxford 1992)
21. Budtz-Jørgensen C, Rev. Sci. Instrum. 63 (1992) 648
22. Bouclier R *et al.*, Nucl. Instrum. and Meth. A323 (1992) 240
23. Bateman JE & Connolly JF, RAL-92-085 (1992)
24. Oed A, Nucl. Instrum. and Meth. A367 (1995) 34
25. Sauli F, CERN/DRDC/93-34 (1993)
26. Sauli F, Nucl. Phys. 61B (1998) 236
27. Proc. Int. Workshop on Micro-Strip Gas Chambers, Legnaro, 1994. Della Mea G & Sauli F, Ed. (Progetto, Padova)
28. Proc. Int. Workshop on Micro-Strip Gas Chambers, Lyon, 1996. Contardo D & Sauli F, Ed. (Medcom Lyon)
29. Florent JJ *et al.*, Nucl. Instrum. and Meth. A329 (1993) 125
30. Bellazzini R & Spezziga MA, Riv. Nuovo Cimento 17 (1994)
31. Biagi SF, Nucl. Instrum. and Meth. A 283 (1989) 716
32. Veenhof R, Nucl. Instum. and Meth. A419 726
33. Angelini F *et al.*, Nucl. Instrum. and Meth. A 382 (1996) 461
34. Bateman JE *et al.*, RAL-95-038 (1995)
35. Bouclier R *et al.*, Nucl. Instrum. and Meth. 367 (1995) 168
36. Fang R *et al.*, Nucl. Instrum. and Meth. A 378 (1996) 439
37. Cicognani G *et al.*, Nucl. Instrum. and Meth. A 392 (1997) 115
38. Frolov AR *et al.*, Nucl. Instrum. and Meth. A307 (1991) 497
39. Minakov GD *et al.*, Nucl. Instrum. and Meth. A326 (1993) 566
40. Bouclier R *et al.*, Nucl. Instrum. and Meth. A332 (1993) 100
41. Bouclier R *et al.*, IEEE Trans. Nucl. Sci. NS-41 (1994) 821
42. Bateman JE *et al.*, Proc. MSGC Workshop, Legnaro (1994) 22
43. Pestov YN & Shekhtman LI, Nucl. Instrum. and Meth. A338 (1994) 368

44. Gerndt EKE *et al.*, Nucl. Instrum. and Meth. A 388 (1997) 42
45. Angelini F & al e, Nucl. Instrum. and Meth. A 314 (1992) 450
46. Pallarès A *et al.*, CRN 95-14 (1995)
47. Della Mea G *et al.*, J. Am. Ceramic Soc. 76 (1993) 2930
48. Della Mea G *et al.*, Thin Solid Films 241 (1994) 25
49. Bouclier R *et al.*, Proc. MSGC Workshop, Legnaro (1994) 39
50. Gong WG *et al.*, Nucl. Instrum. and Meth. A360 (1994) 30
51. Bateman JE *et al.*, RAL-TR-95-032 (1995)
52. Bouclier R *et al.*, Nucl. Instrum. and Meth. A 369 (1996) 328
53. Boimska B *et al.*, Nucl. Instrum. and Meth. A400 (1997) 9
54. Boimska B *et al.*, Nucl. Instrum. and Meth. A404 (1997) 57
55. Barr A *et al.*, Nuclear Physics B 61 B (1996) 315
56. Zeuner T, Nucl. Instrum. and Meth. A 392 (1997) 105
57. Savard P *et al.*, Nucl. Instrum. and Meth. A 337 (1993) 125
58. Bagulya AV *et al.*, Proc. MSGC Workshop, Lyon (1995) 243
59. Cho HS *et al.*, Nucl. Instrum. and Meth. A 401 (1997) 81
60. Buzulutskov A *et al.*, Nucl. Instrum. and Meth. A409 (1998) 33
61. Salomon M *et al.*, TRI-PP 94-24 (1994)
62. Brons S *et al.*, Nucl. Instrum. and Meth. A342 (1994) 411
63. Bouclier R *et al.*, IEEE Trans. Nucl. Science NS-43 (1996) 1220
64. Stahl H *et al.*, Nucl. Instrum. and Meth. A297 (1990) 95
65. Schmidt S *et al.*, Nucl. Instrum. and Meth. A 337 (1994) 382
66. Dixit M *et al.*, Nucl. Instrum. and Meth. A348 (1994) 365
67. Salomon M *et al.*, IEEE Trans. Nucl. Sci. NS-41 (1994) 817
68. Salomon M *et al.*, IEEE Trans. Nucl. Sci. NS-43 (1996) 1157
69. Bouclier R *et al.*, Nucl. Instrum. and Meth. A365 (1995) 65
70. Beckers T *et al.*, Nucl. Instrum. and Meth. A346 (1994) 95
71. Bateman JE & Connolly JF, RAL-94-114 (1994)
72. Brom JM *et al.*, CRN 95-14 (1995)
73. Bouhali O *et al.*, Nucl. Instrum. and Meth. A 378 (1996) 432
74. Jelen K *et al.*, Nucl. Instrum. and Meth. A 392 (1997) 80
75. van Hunen JJ, Nucl. Instrum. and Meth. A 409 (1998) 95
76. Bohm J *et al.*, Nucl. Instrum. and Meth. A360 (1995) 34
77. Kiourkos S *et al.*, Nucl. Instrum. and Meth. A348 (1994) 351
78. Snow S *et al.*, Proc. MSGC Workshop, Lyon (1995) 127
79. Pooth O, Nucl. Instrum. and Meth. A 419 (1998) 375
80. Bouhali O *et al.*, Proc. MSGC Workshop, Lyon (1995) 101
81. Barthe S *et al.*, Proc. MSGC Workshop, Lyon (1995) 107
82. Duerdoth I *et al.*, Nucl. Instrum. and Meth. A348 (1994) 356
83. Mack V *et al.*, Nucl. Instrum. and Meth. A 367 (1995) 173
84. Angelini F *et al.*, Proc. LHC Workshop (Aachen) 222
85. Geijsberts M *et al.*, Nucl. Instrum. and Meth. A313 (1992) 377
86. Dixit MS *et al.*, Proc. MSGC Workshop, Legnaro (1994) 138
87. Bouhali O *et al.*, IISN0379-301X (1996)
88. Amos N *et al.*, Nucl. Instrum. and Meth. A 384 (1997) 342
89. Gómez F *et al.*, Nucl. Instrum. and Meth. A 384 (1997) 351
90. Barr A *et al.*, Nucl. Instrum. and Meth. A 392 (1997) 99
91. Barr A *et al.*, Nucl. Instrum. and Meth. A403 (1998) 31
92. Abbaneo D *et al.*, Nucl. Instrum. and Meth. A 409 (1998) 37
93. Bachman S *et al.*, Nucl. Instrum. and Meth. A 409 (1998) 6
94. Albert E *et al.*, Nucl. Instrum. and Meth. A 409 (1998) 70

95.   Ballintijn MK *et al.*, NIKHEF 95-002 (1995)
96.   Henkes T *et al.*, Proc. MSGC Workshop, Lyon (1995) 143
97.   de Groot N *et al.*, Proc. MSGC Workshop, Lyon (1995) 137
98.   Blouw J *et al.*, Proc. MSGC Workshop, Lyon (1995) 143
99.   Landry M *et al.*, Subm. Nucl. Instrum. and Meth. (1998)
100.   Hall G, Proc. MSGC Workshop, Lyon (1994) 165
101.   Bouclier R *et al.*, Proc. MSGC Workshop, Legnaro (1994) 79
102.   Clergeau J-F *et al.*, Nucl. Instrum. and Meth. A 392 (1997) 109
103.   Schmitz J, Nucl. Instrum. and Meth. A323 (1992) 638
104.   Angelini F *et al.*, Nucl. Physics 23 A (1991) 254
105.   van den Berg FD *et al.*, Nucl. Instrum. and Meth. A349 (1994) 438
106.   Abbaneo D & al e, CERN-CMS CR 1998/012 (1998)
107.   Baiboussinov B *et al.*, CMS TN/95-201 (1995)
108.   Cicognani G *et al.*, IEEE Trans. Nucl. Sci. NS-45 (1998) 249
109.   Vellettaz N *et al.*, Nucl. Instrum. and Meth. A 392 (1997) 73
110.   Vellettaz N *et al.*, Proc. MSGC Workshop, Lyon (1995) 73
111.   Capeáns M *et al.*, Nucl. Phys. B 61B (1998) 17
112.   Angelini F *et al.*, Nucl. Instrum. and Meth. A283 (1989) 755
113.   Angelini F *et al.*, Nucl. Instrum. and Meth. A323 (1992) 229
114.   Nagae T *et al.*, Nucl. Instrum. and Meth. A323 (1992) 236
115.   Tanimori T *et al.*, Nucl. Instrum. and Meth. A381 (1996) 280
116.   Ochi A *et al.*, Nucl. Instrum. and Meth. A 392 (1997) 124
117.   Peskov V *et al.*, Nucl. Instrum. and Meth. A397 (1997) 243
118.   Peskov V *et al.*, IEEE Trans. Nucl. Sci. NS-45 (1998) 244
119.   Schmidt B, Nucl. Instrum. and Meth. A 419 (1998) 230
120.   Bressan A *et al.*, CERN-EP/98-139. Subm. Nucl. Instrum. and Meth. (1998)
121.   Keller S *et al.*, Nucl. Instrum. and Meth. A 419 (1998) 382
122.   Fonte P *et al.*, Nucl. Instrum. and Meth. A 419 (1998) 405
123.   Cho HS *et al.*, IEEE Trans. Nucl. Sci. NS-44 (1997) 635
124.   Cho HS *et al.*, IEEE Trans. Nucl. Sci. NS-45 (1998) 280
125.   Schmidt B, Proc. Workshop on New Detectors (Erice)
126.   Bellazzini R *et al.*, Nucl. Instrum. and Meth. A398 (1998) 426
127.   Va'vra J, Proc. Workshop on Radiation Damage to Wire Chambers (Berkeley) 263
128.   Va'vra J, Nucl. Instrum. and Meth. A323 (1992) 34
129.   Bouclier R *et al.*, Nucl. Instrum. and Meth. A350 (1994) 464
130.   Bouclier R *et al.*, Nucl. Instrum. and Meth. A381 (1996) 289
131.   Bouclier R *et al.*, Proc. MSGC Workshop, Legnaro (1994) 48
132.   Duerdoth IP *et al.*, Nucl. Instrum. and Meth. A 392 (1997) 127
133.   van den Berg FD *et al.*, Nucl. Instrum. and Meth. A 392 (1997) 94
134.   Schefer J *et al.*, Proc. MSGC Workshop, Legnaro (1994) 173
135.   Ramsey BD *et al.*, Proc. SPIE 1994 Int. Symp. on Optical Applied Science and Engineering (San Diego) 31
136.   Dixit MS *et al.*, IEEE Trans. Instrum. and Meas. IMTC/97 (1997)
137.   Zhukov V *et al.*, Nucl. Instrum. and Meth. A 392 (1997) 83
138.   Gebauer B *et al.*, Nucl. Instrum. and Meth. A 392 (1997) 68
139.   Gebauer B *et al.*, Nucl. Instrum. and Meth. A 409 (1998) 56
140.   Breskin A *et al.*, Nucl. Instrum. and Meth. A 345 (1994) 205
141.   Zeitelhack K *et al.*, Proc. MSGC Workshop, Lyon (1995) 53
142.   Anderson DF *et al.*, Nucl. Phys. B 44 (1995) 213
143.   Eckardt V *et al.*, Proc. MSGC Workshop, Legnaro (1994) 184

144. Frankenfeld U & Sann H, Proc. MSGC Workshop, Lyon (1995) 85
145. Baru SE *et al.*, Proc. MSGC Workshop, Lyon (1995) 27
146.   Geltenbort P & Oed A, Proc. European Workshop on X-ray Detectors for Synchrotron Radiation Sources (Assois) 107
147. Geltenbort P & Oed A, Proc. SPIE's 1992 Int. Symp. on Optical Applied Science and Engineering (San Diego)
148. Akimov D *et al.*, Proc. MSGC Workshop, Legnaro (1994) 215
149. Policarpo AJP *et al.*, Nucl. Instrum. and Meth. A365 (1995) 568
150. Angelini F *et al.*, Nucl. Instrum. and Meth. A335 (1993) 69
151. Angelini F *et al.*, Nucl. Instrum. and Meth. A 349 (1995) 273
152. Angelini A *et al.*, Proc. MSGC Workshop, Lyon (1995) 307
153. van den Berg FD *et al.*, Nucl. Instrum. and Meth. A 409 (1998) 90
154. Biagi SF *et al.*, Nucl. Instrum. and Meth. A 392 (1997) 131
155. Angelini F *et al.*, Proc. MSGC Workshop, Lyon (1995) 91
156. Bellazzini R *et al.*, Nucl. Instrum. and Meth. A 409 (1998) 14
157. Cho HS *et al.*, IEEE Trans. Nucl. Sci. NS-44 (1997) 747
158. Fraga FAF *et al.*, Nucl. Instrum. and Meth. A 392 (1997) 135
159. Fraga FAF *et al.*, Nucl. Instrum. and Meth. A 419 (1998) 460
160. Clergeau J-F *et al.*, Nucl. Instrum. and Meth. A 392 (1997) 140
161. Chorowicz V *et al.*, Nucl. Instrum. and Meth. A 401 (1997) 238
162. Biagi SF *et al.*, Nucl. Instrum. and Meth. A371 (1995) 12
163. Biagi S *et al.*, Nucl. Instrum. and Meth. A 419 (1998) 438
164. Biagi SF *et al.*, Subm. Nucl. Instr. and Meth. (1998)
165. Breskin A *et al.*, Nucl. Instrum. and Meth. A394 (1997) 21
166. Fonte P *et al.*, Nucl. Instrum. and Meth. A305 (1991) 91
167. Fonte P, IEEE Trans. Nucl. Sci. NS-43 (1996) 2135
168. Ivaniouchenkov I *et al.*, IEEE Trans. Nucl. Sci. NS-45 (1998) 258
169. Giomataris Y, Nucl. Instrum. and Meth. A 419 (1998) 239
170. Derré J *et al.*, Subm. Nucl. Instrum. and Meth. (1998)
171. Cussonneau JP *et al.*, Nucl. Instrum. and Meth. A 419 (1998) 452
172. Schmitz J, NIKHEF-H/91-14 (1991)
173. Jeavons A *et al.*, Nucl. Instrum. and Meth. 176 (1980) 89
174. Sarvestrani A *et al.*, Nucl. Instrum. and Meth. A 419 (1998) 444
175. Sarvestani A *et al.*, Proc. MSGC Workshop, Lyon (1995) 45
176. Charpak G & Sauli F, Phys. Letters 78 B (1978) 523
177. Adams M *et al.*, Nucl. Instrum. and Meth. 217 (1983) 237
178. Bouclier R *et al.*, Nucl. Instrum. and Meth. A396 (1997) 50
179. Beaumont W *et al.*, Nucl. Instrum. and Meth. A 419 (1998) 394
180. Benhammou Y *et al.*, Nucl. Instrum. and Meth. A 419 (1998) 400
181. Benlloch J *et al.*, IEEE Trans. Nucl. Sci. NS-45 (1998) 234
182. Büttner C *et al.*, Nucl. Instrum. and Meth. A 409 (1998) 79
183. Benlloch J *et al.*, Nucl. Instrum. and Meth. A 419 (1998) 410
184. Bressan A *et al.*, CERN-EP/98-163. Subm. Nucl. Instrum. and Meth. (1998)
185. Bressan A *et al.*, CERN-EP/98-164. Subm. Nucl. Instrum. and Meth. (1998)
186. Bressan A *et al.*, BINP 98-59. Subm. Nucl. Instrum. and Meth. (1998)
187. Chechik R *et al.*, Subm. Nucl. Instrum. and Meth. (1998)
188. Buzulutskov A *et al.*, Subm. Nucl. Instrum. and Meth. (1998)
189. Garty G *et al.*, Subm. Nucl. Instrum. and Meth. (1998)
190. Va'vra J *et al.*, Subm. Nucl. Instrum. and Meth. (1998)

FIGURE CAPTIONS

Figure 1: Close view of one of the first micro-strip plates developed by Oed at ILL.
Figure 2: Equi-potentials and field lines in the region of the strips. The back-plane potential has been selected to prevent field lines to enter the dielectric.
Figure 3: Typical charge profile on anode strips for a localized avalanche. The positive overshoot is due to a signal re-injection from the grouped cathode strips.
Figure 4: Electric field component parallel to the substrate and close to the surface. The full curve is computed for an insulating support, the dashed curve for a support with a thin, lower resistivity coating.
Figure 5: Field lines and equi-potentials computed for a back-plane voltage close to the cathode. Field lines enter the dielectric, inducing charging-up processes.
Figure 6: Schematics of two photo-lithographic methods used for MSGC manufacturing: direct etching (a) and lift-off (b).
Figure 7: Initial gain variation at power-on for a plate made on insulating support.
Figure 8: Relative gain as a function of irradiation rate for a MSGC made on boro-silicate glass. The detailed evolution depends strongly on the applied voltages.
Figure 9: Relative gain as a function of irradiation rate for MSGC plates manufactured on electron-conducting glass in a range of resistivity.
Figure 10: Relative gain as a function of rate for two MSGC plates manufactured on glass coated with low-resistivity diamond-like carbon.
Figure 11: Gain and maximum gain measured with a set of plates in a range of cathode strip width.
Figure 12: Examples of absolute gain measured in several gas mixtures.
Figure 13: Schematics of the light mechanical assembly of a MSGC module.
Figure 14: An eight-plate module, complete with read-out electronics, developed for the CMS Forward MSGC detector.
Figure 15: Total charge spectrum recorded for minimum ionizing tracks in a three mm thick MSGC.
Figure 16: Detection efficiency plateaux for minimum ionizing particles as a function of cathode voltage in several gas mixtures.
Figure 17: Localization accuracy (rms) as a function of angle of incidence. The curves correspond to different reconstruction algorithms.
Figure 18: Example of two-dimensional imaging capability. The MSGC with back-plane readout was exposed to a thermal neutron flux through a mask.
Figure 19: Close view of the strips damaged by discharges.
Figure 20: Gain curve, measured at low irradiation rate, and discharge probability under irradiation of an internal a emitter.
Figure 21: Comparison of aging rate under irradiation for identical plates mounted in a conventional fiberglass assembly, and in a clean container.
Figure 22: Aging rates under irradiation of plates manufactured on insulating and semi-conducting support, and with different metals.
Figure 23: Using clean construction materials and gases, plates made on electro-conducting glass do not show any deterioration of performance under irradiation up to a total collected charge of 100 mC cm^{-1}.
Figure 24: Schematics and electric field structure in the micro-gap chamber.
Figure 25: Two variants of small gap chambers, making use of thick polyimide ridges to prevent the onset of discharges.
Figure 26: Schematics of the micro-dot chamber.
Figure 27: Examples of the very high gains attained with the micro-dot detector in various gas mixtures.

Figure 28: Schematics and electric field map in micromegas.
Figure 29: Detected current with micromegas, measured at increasing flux of ionizing particles.
Figure 30: Maximum gain in micromegas at increasing X-ray flux.
Figure 31: Schematics and fields in the "compteur à trous", CAT.
Figure 32: Example of the energy resolution obtained for 5.4 keV X-rays with CAT.
Figure 33: Close view of the hole structure in the gas electron multiplier.
Figure 34: Field lines and equi-potentials in GEM.
Figure 35: Combined gain curves of a cascaded GEM+MSGC detector.
Figure 36: A large size GEM built for the HERA-B experiment.
Figure 37: Effective gain curves measured with the single GEM+PCB detector in argon-CO_2 mixtures.
Figure 38: Combined gain plot measured with a double-GEM+PCB detector, as a function of voltages applied on each GEM. The dashed line is the discharge limit at an X-ray flux of $5 \cdot 10^5$ mm^{-2}s^{-1}.
Figure 39: Detected currents in the GEM+PCB detector under uniform irradiation, as a function of transfer field.
Figure 40: Efficiency and position accuracy for minimum ionizing particles measured with the double-GEM+PCB detector.
Figure 41: Schematics of a GEM detector with two-dimensional printed circuit board readout.
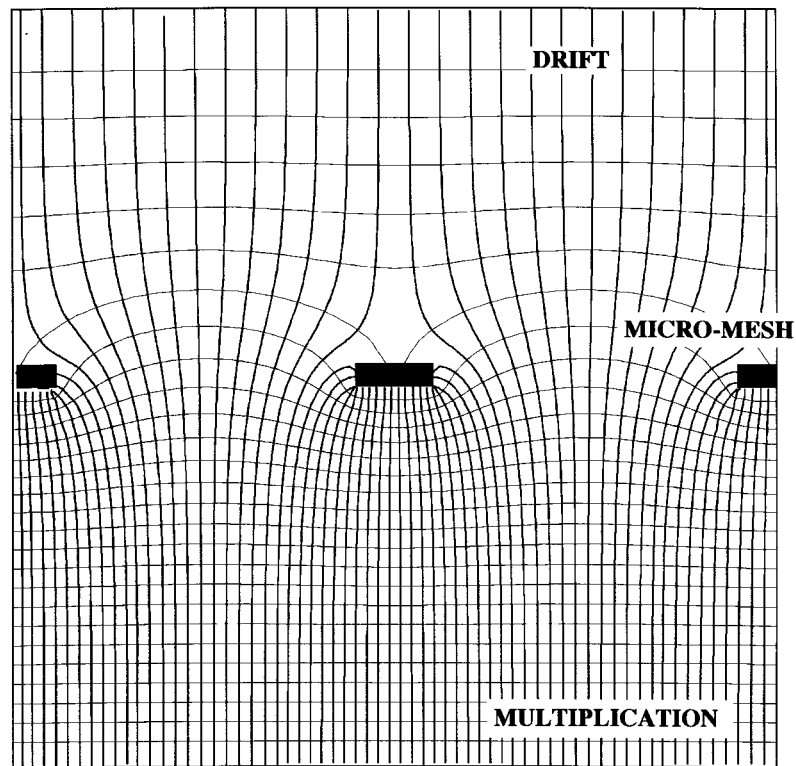Figure 42: Example of the bi-dimensional imaging capability of the GEM+PCB detector: absorption radiography of a micro-mammal foot. The image size is 9x7 mm^2.
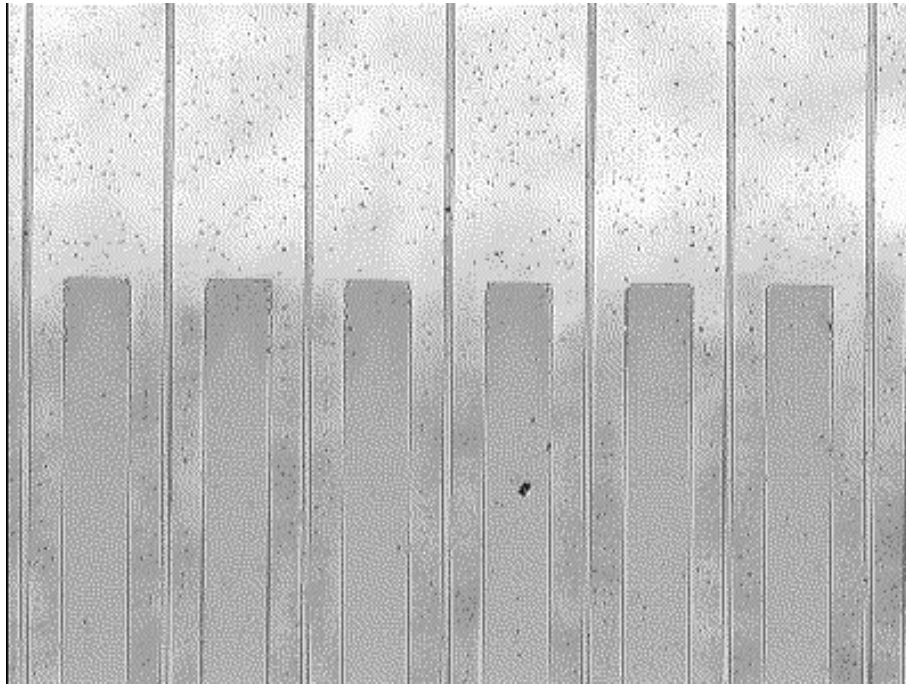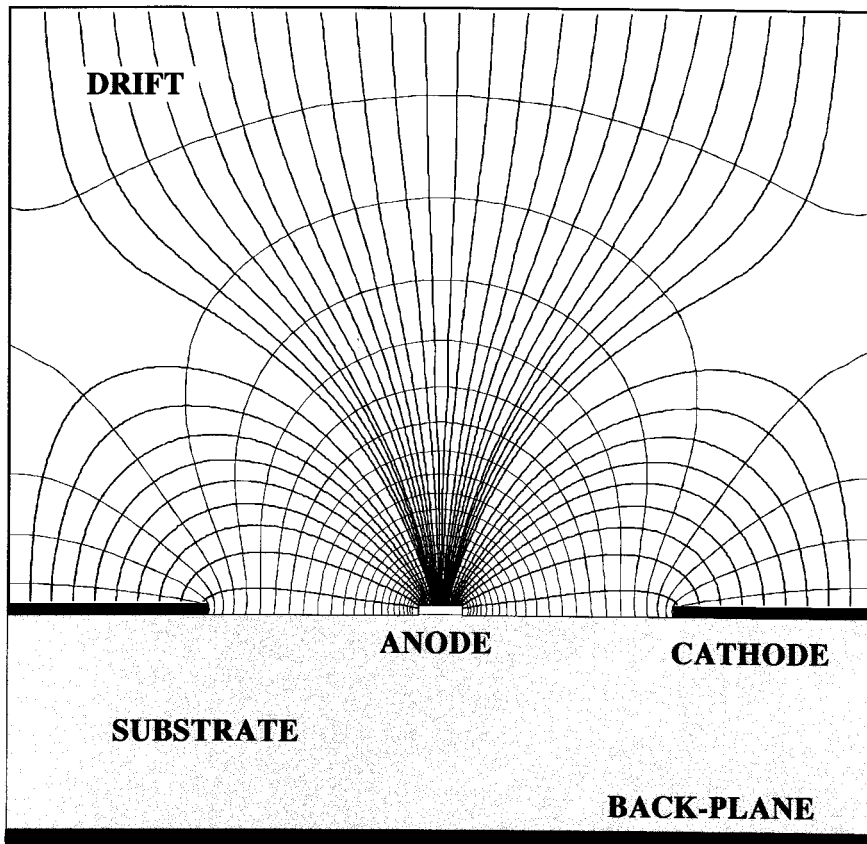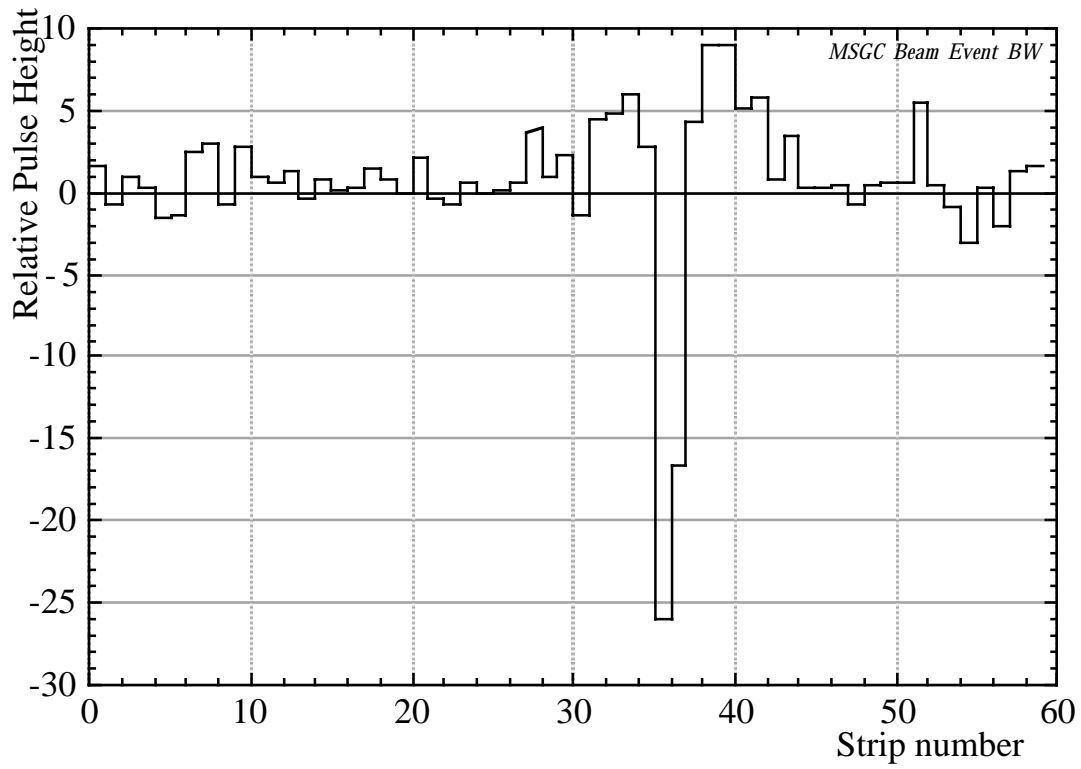
Fig. 1
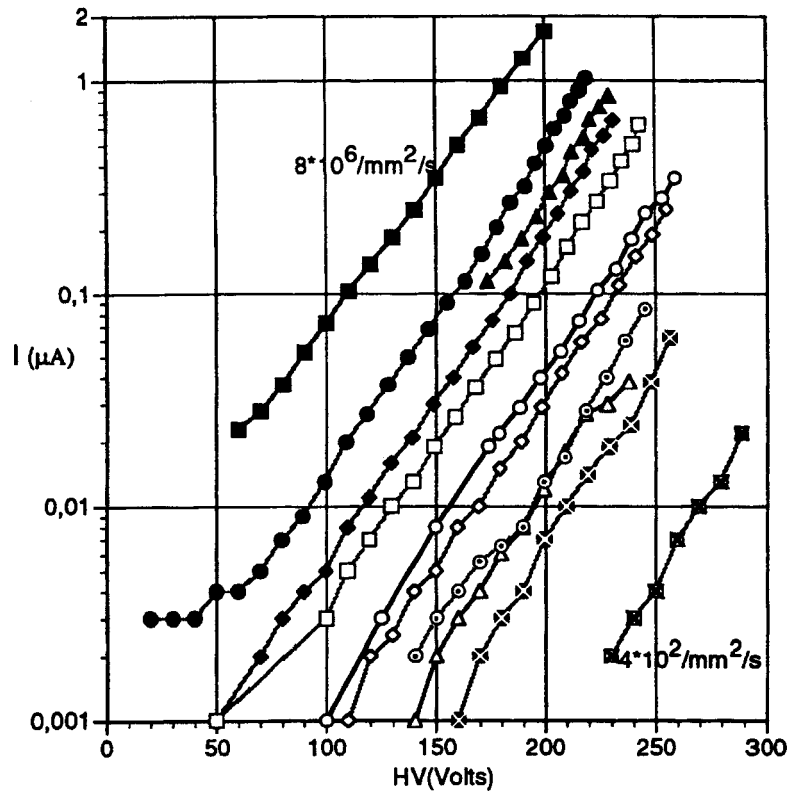

Fig. 2

Fig. 3

Fig. 4

Fig. 5

Fig. 6

Fig. 7

Fig. 8

Relative Gain

Pestov
10^9 Ω cm

S8900
$2 \cdot 10^{12}$ Ω cm

Pestov
10^{12} Ω cm

Rate (mm^{-2}s^{-1})

Fig. 9

Relative Gain

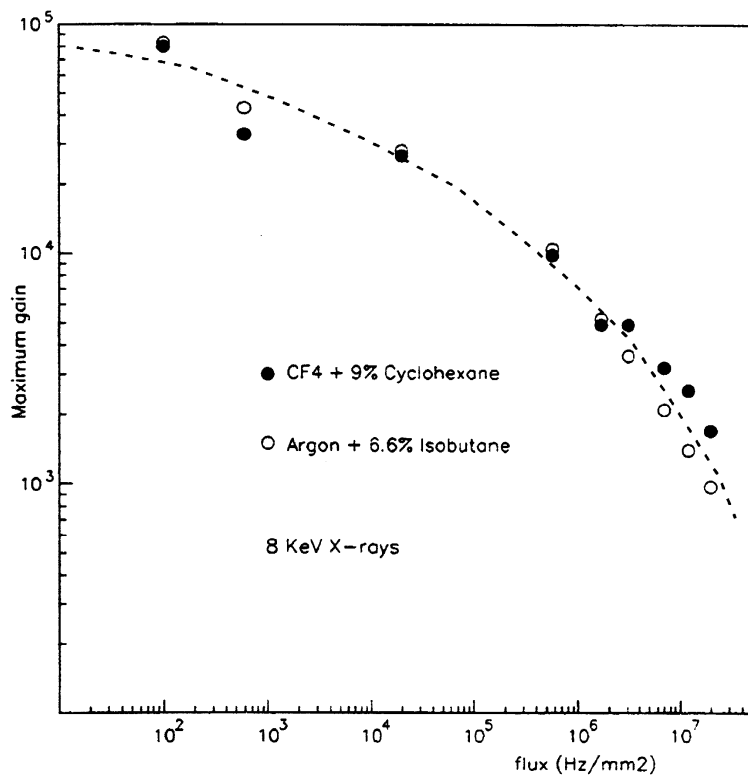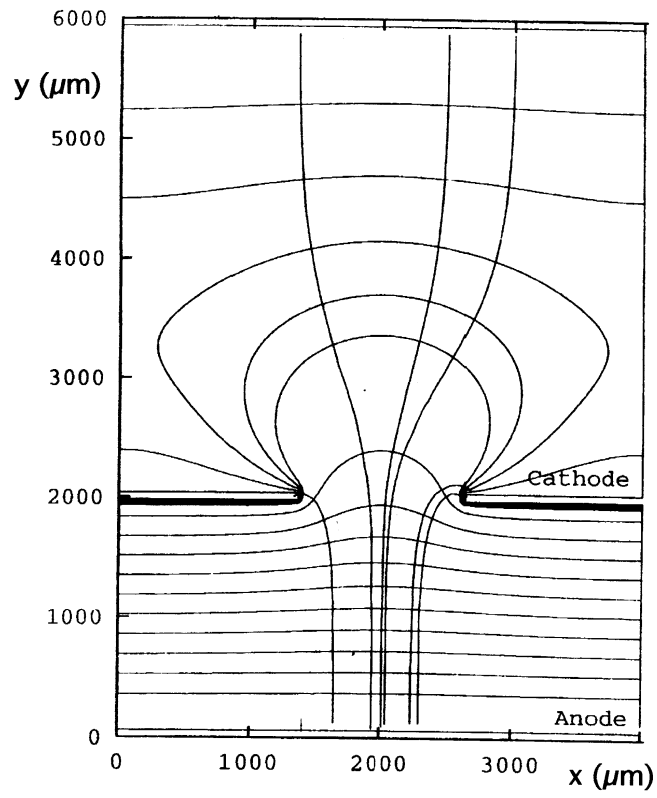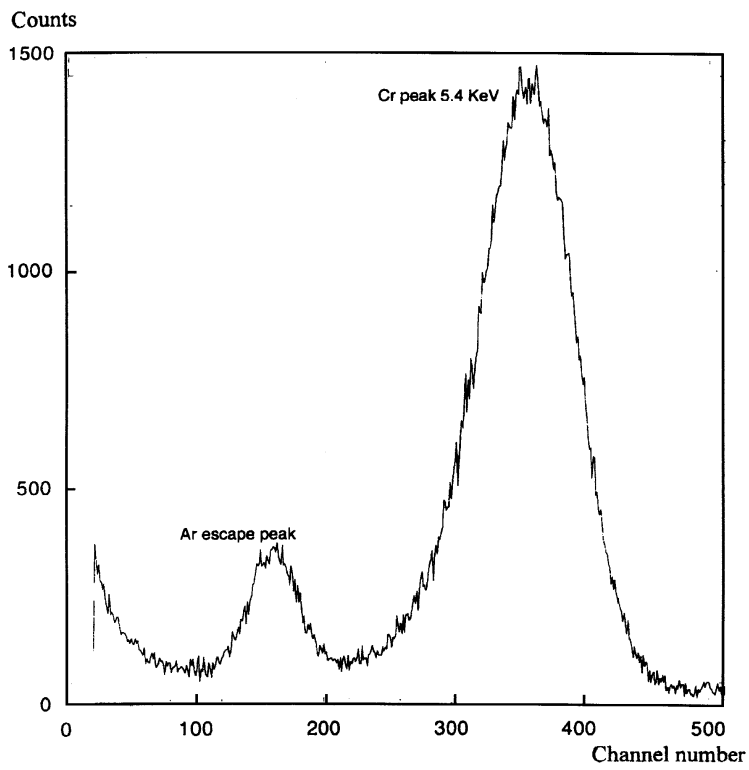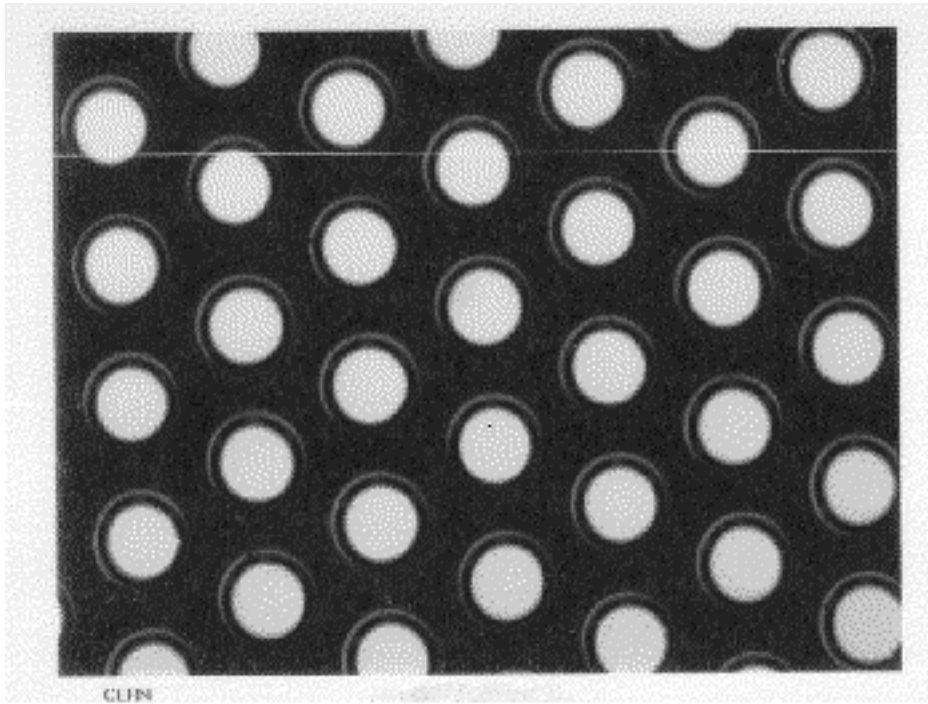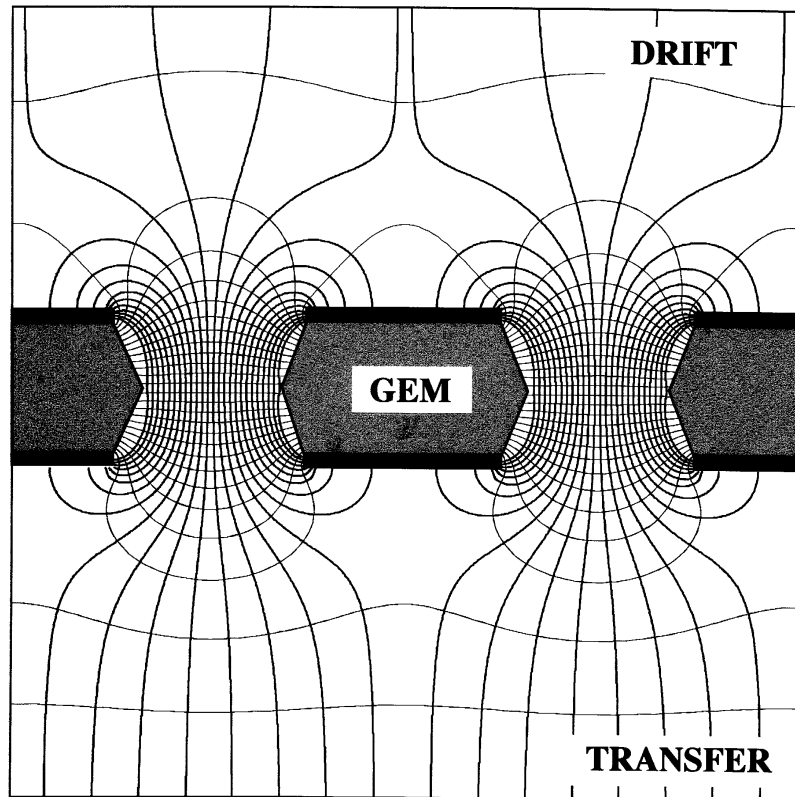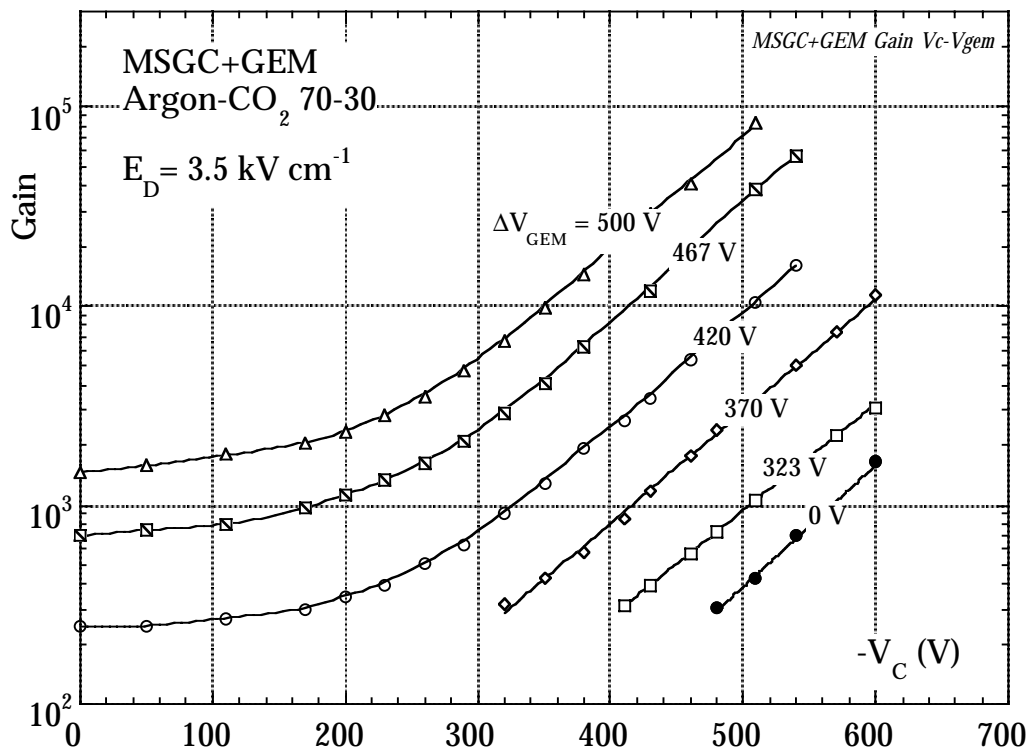• ⟶ Chromium on Diamond-coated D-263
△ ⟶ Gold on Diamond-coated D-263
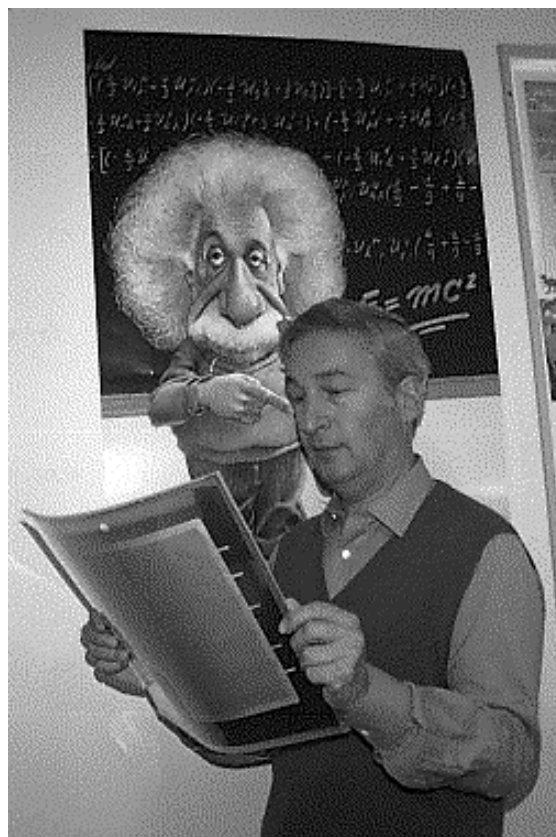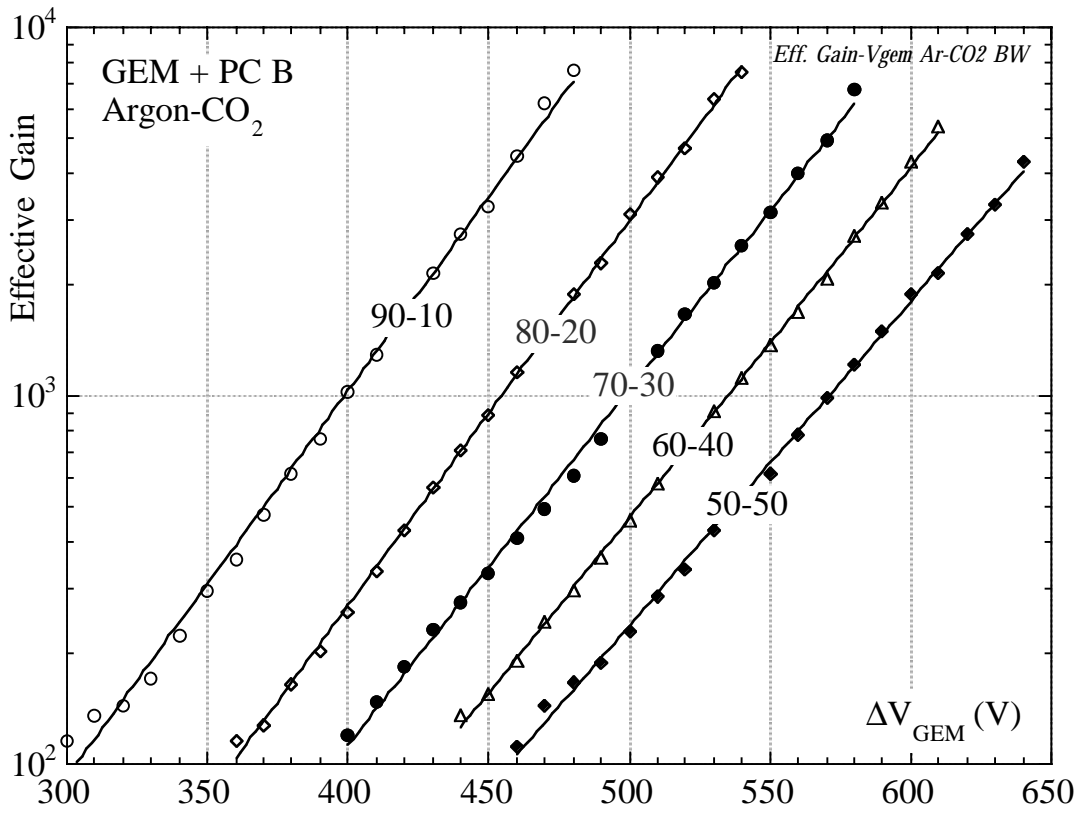
Rate (Hz mm^{-2})
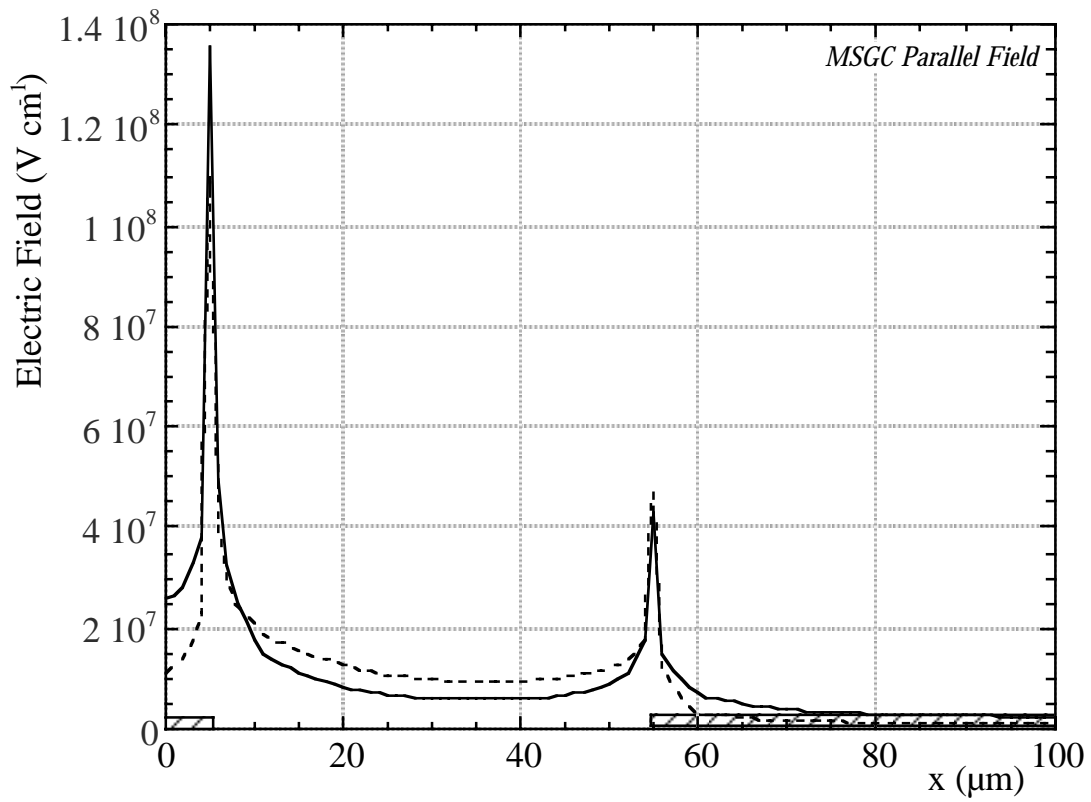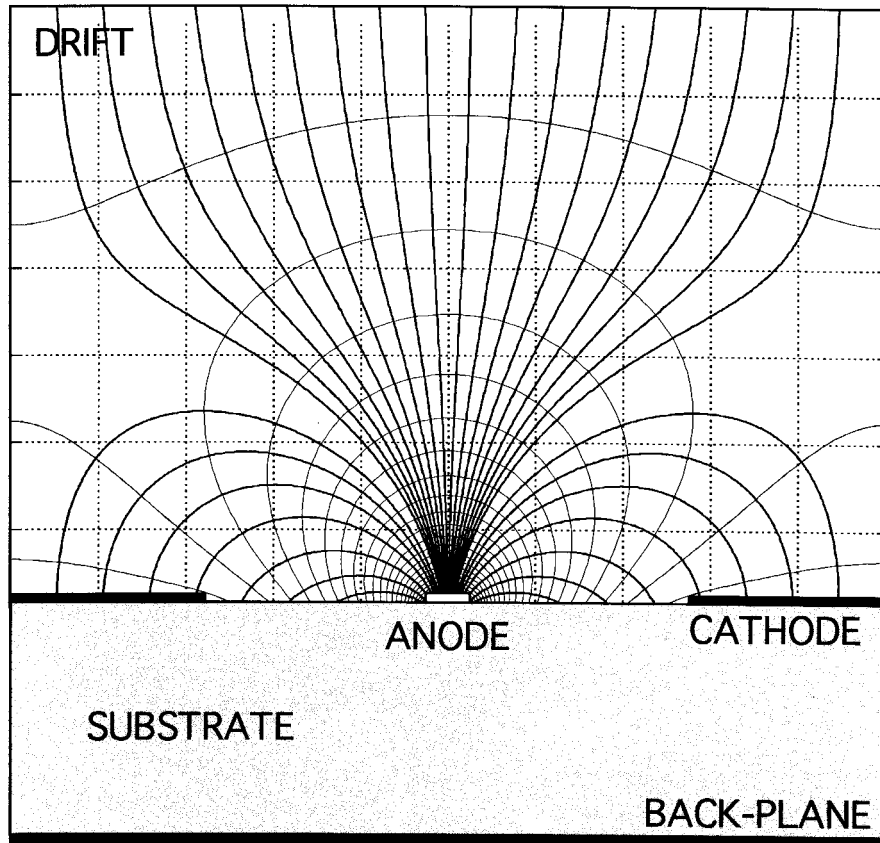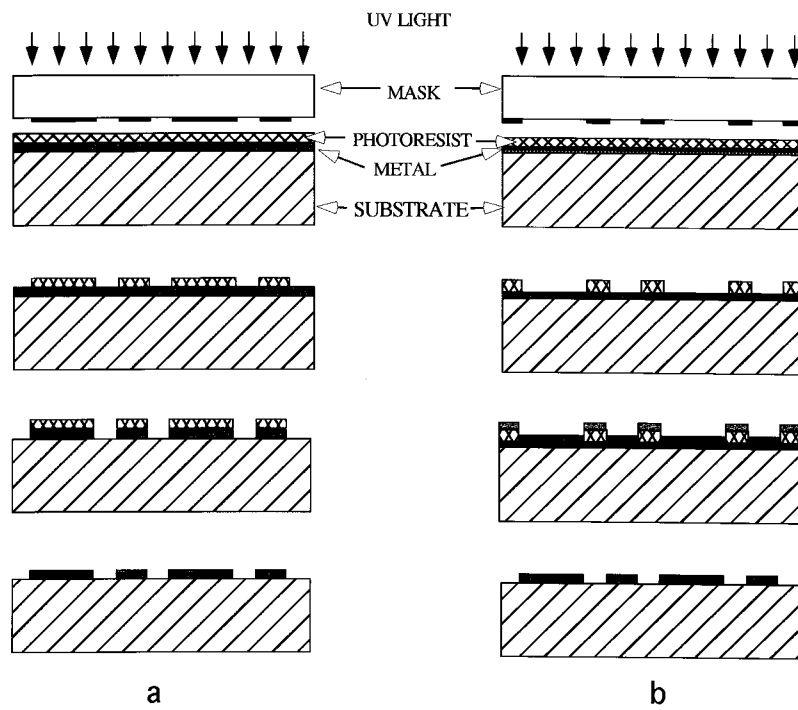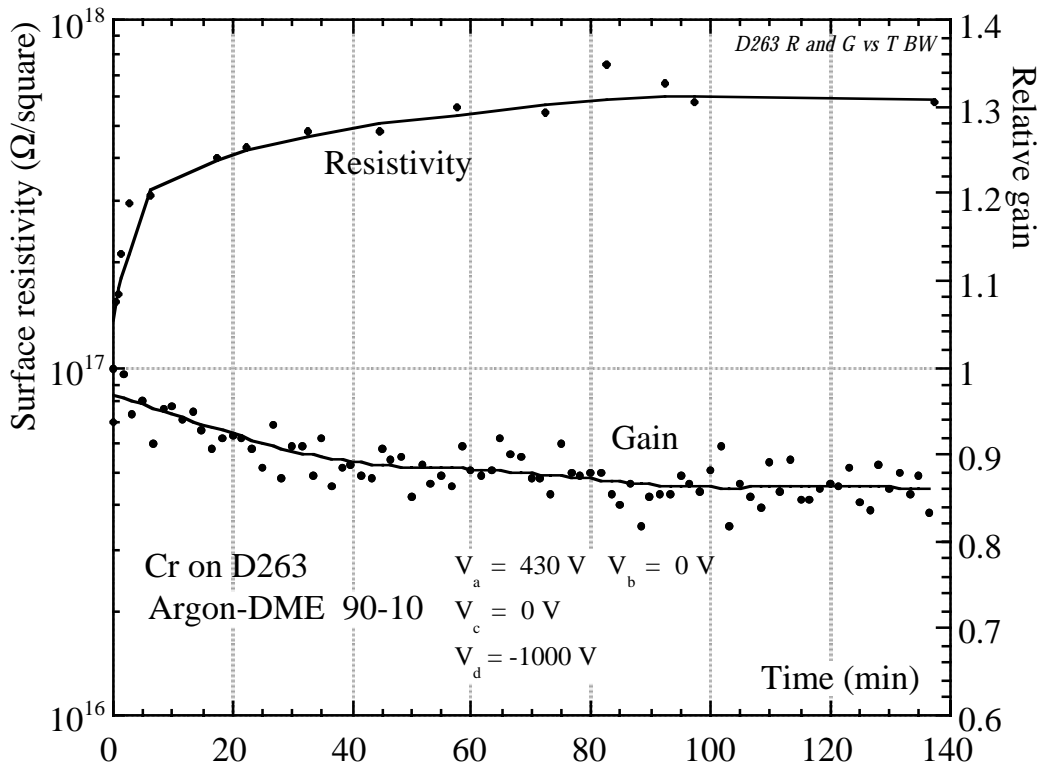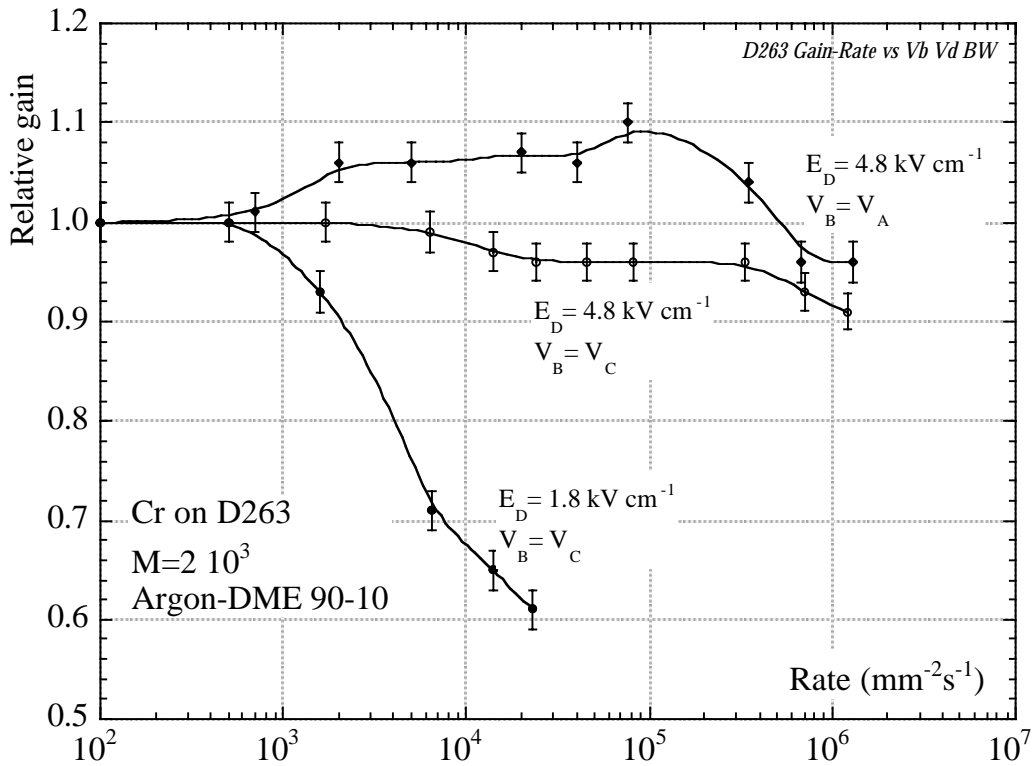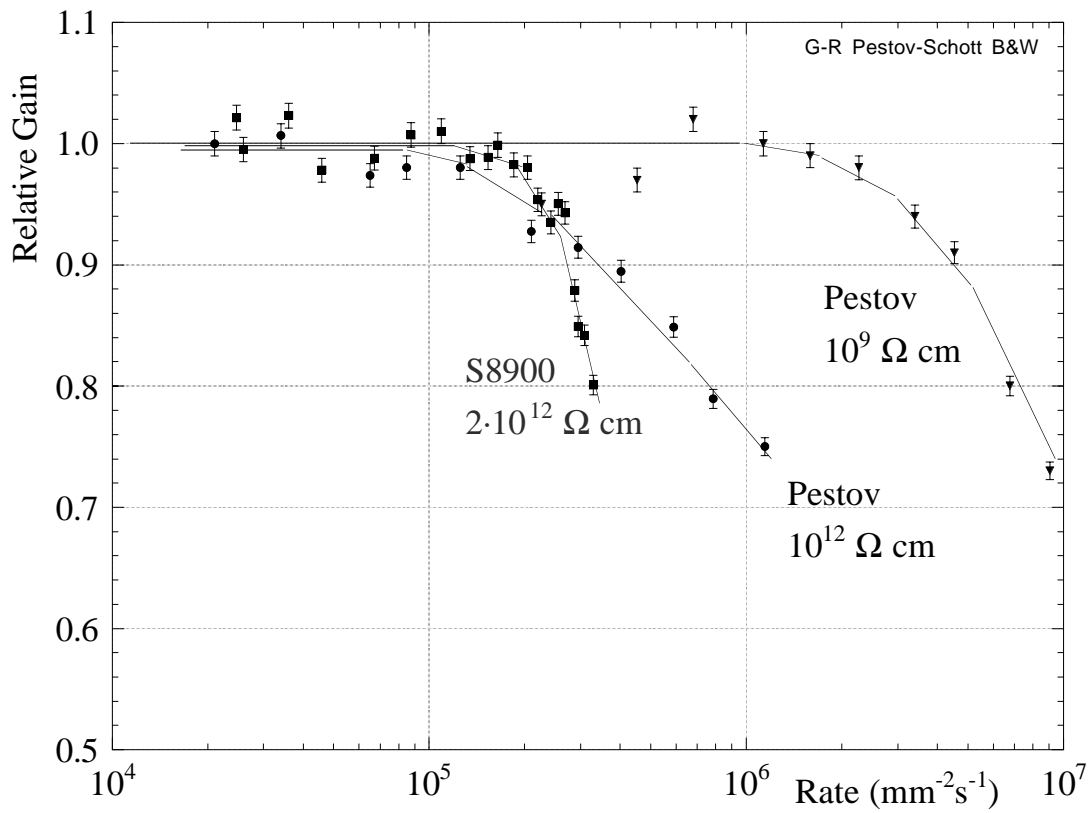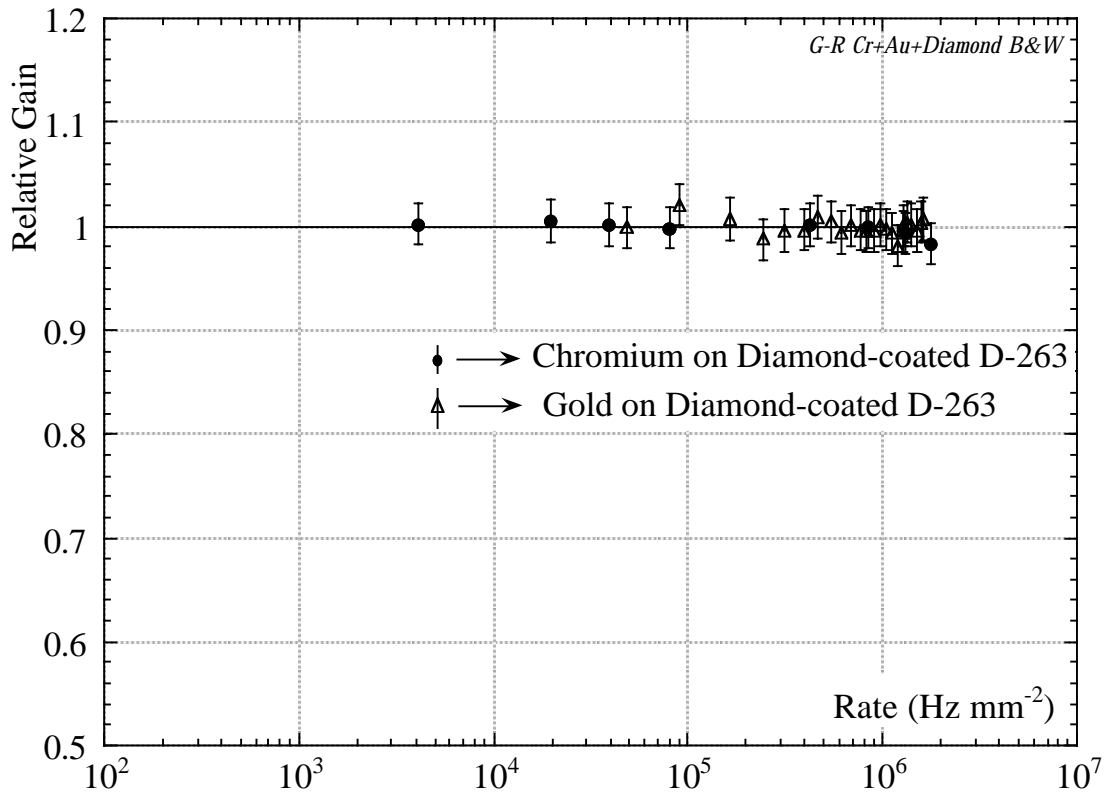
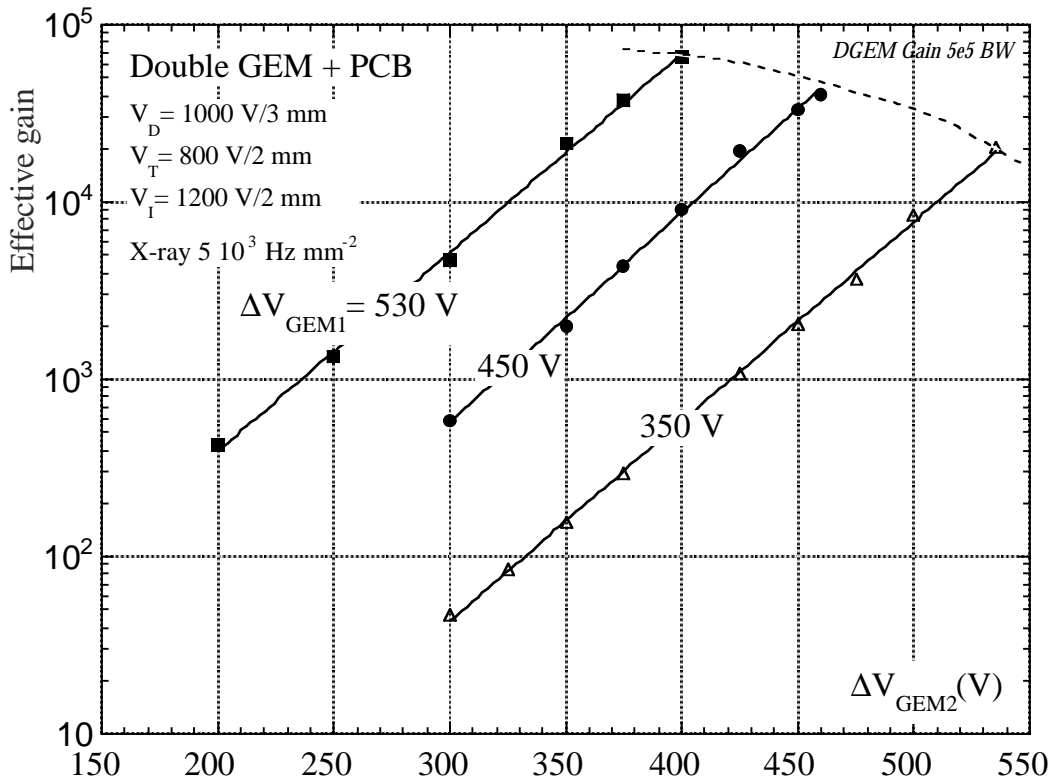Fig. 10
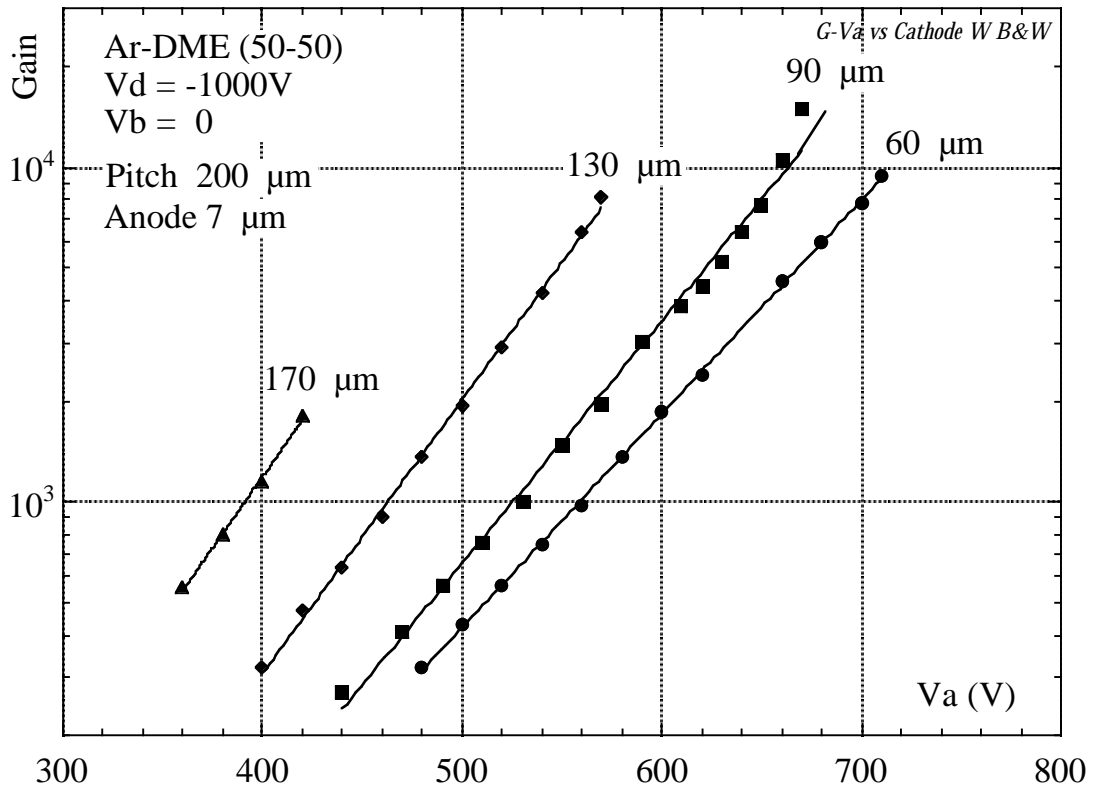
Fig. 11
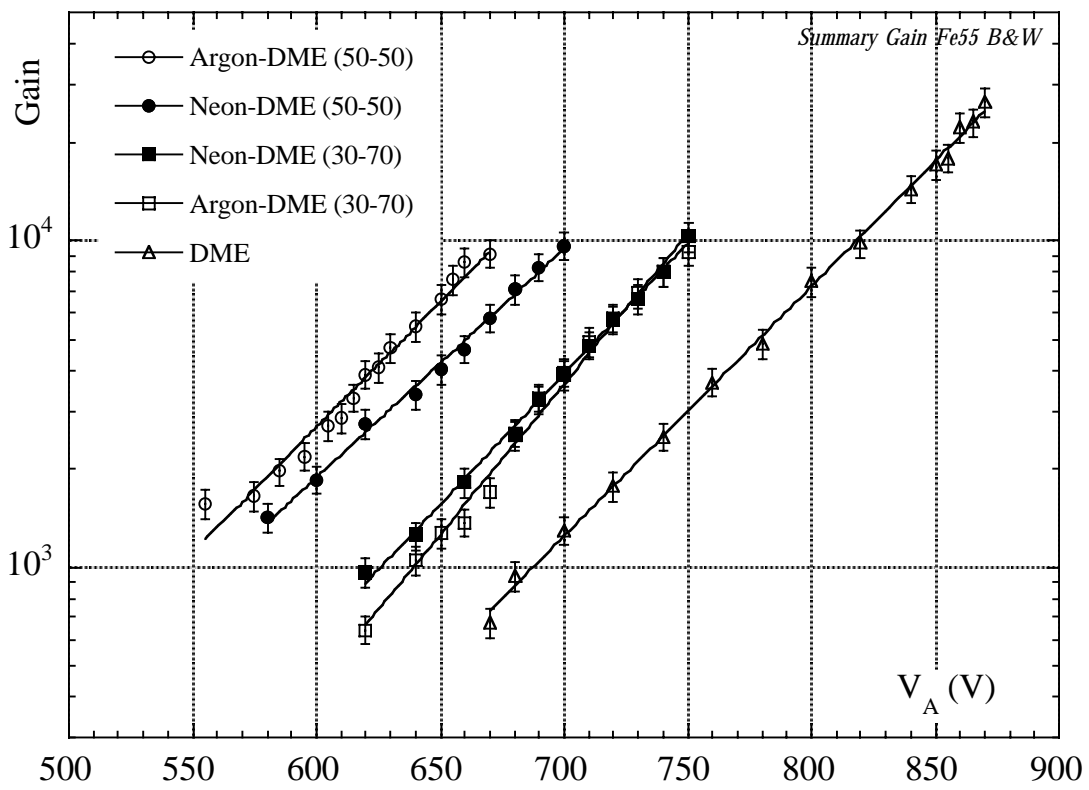
Fig. 12
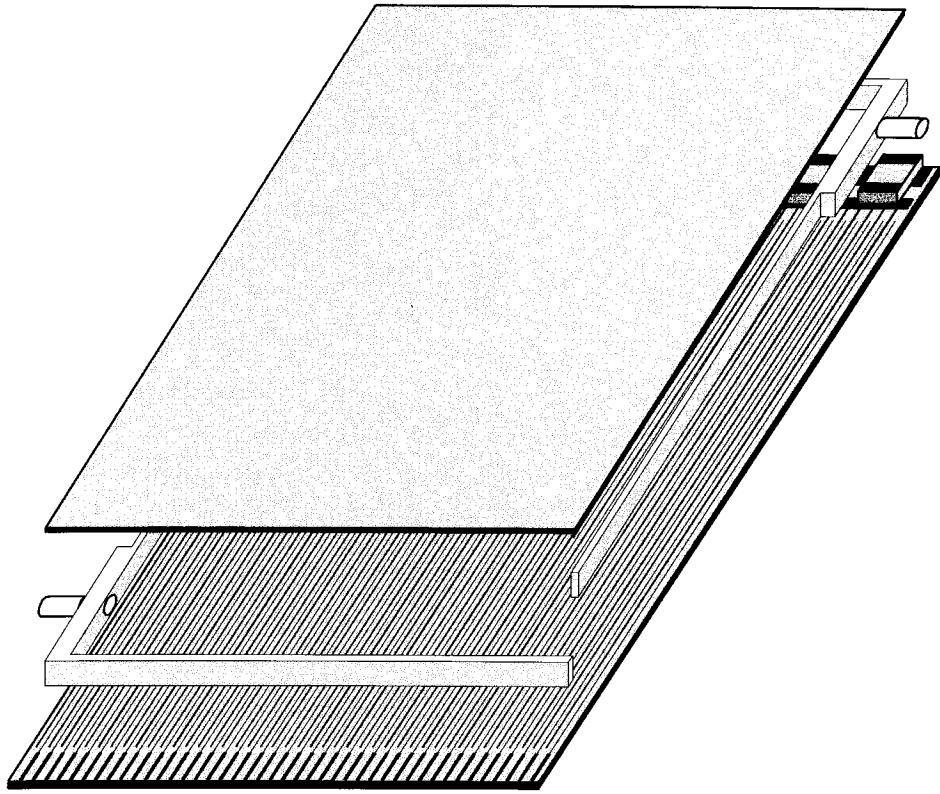
Fig. 13
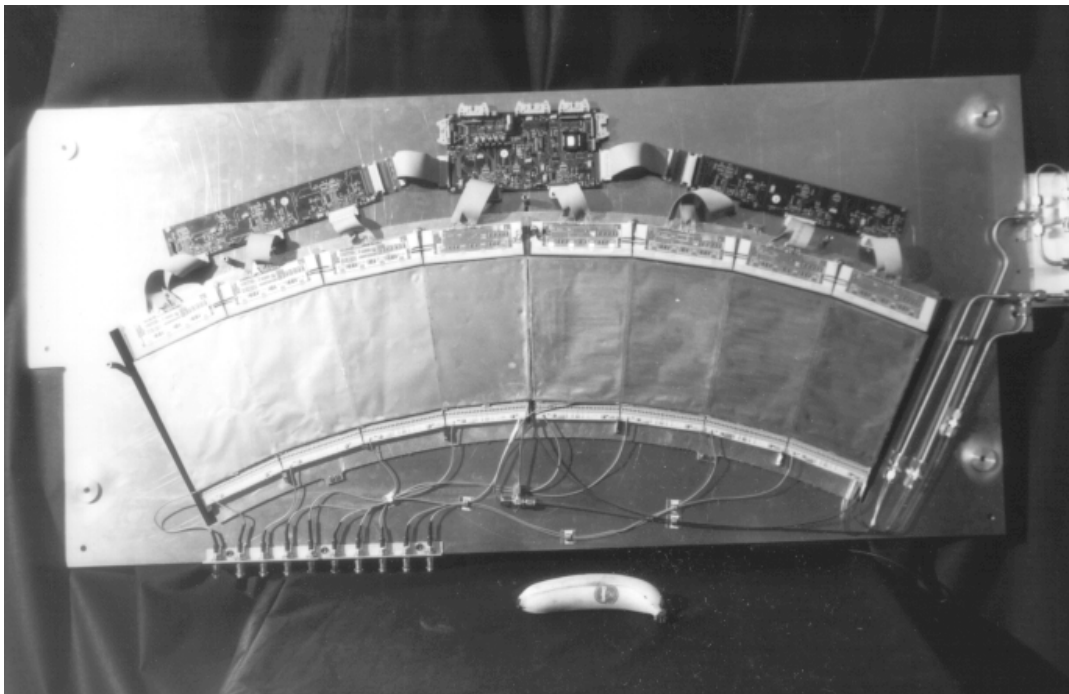
Fig. 14
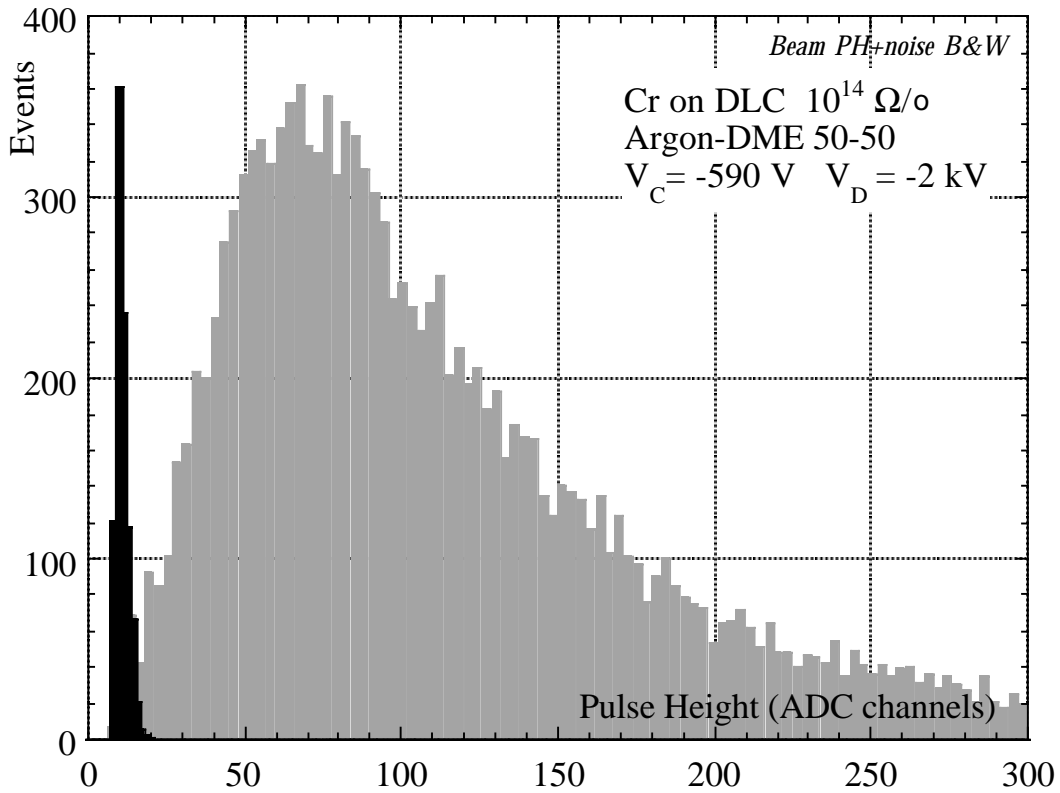
Fig. 15
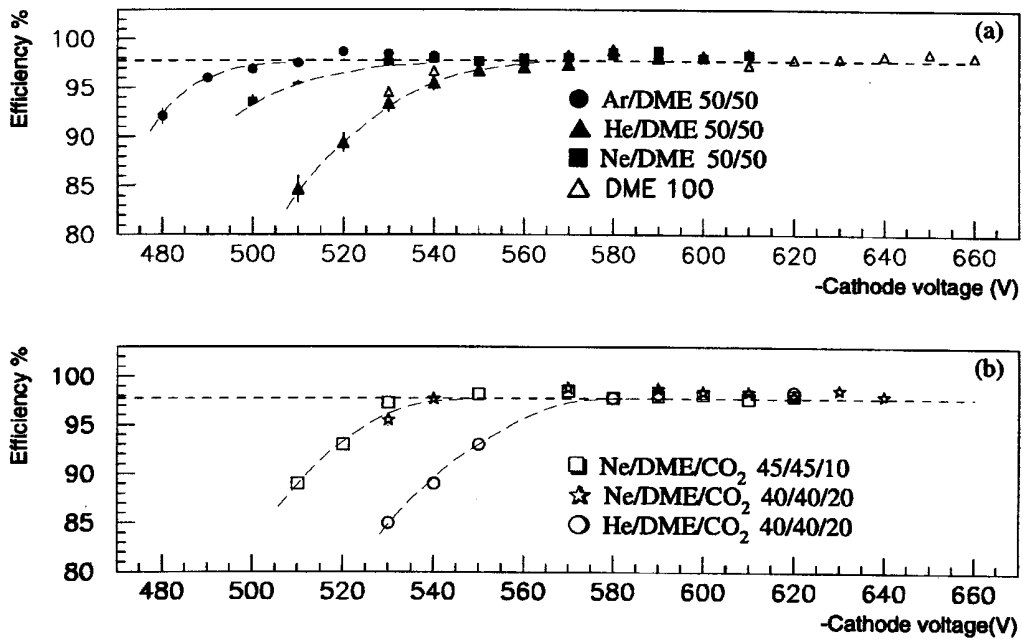
Fig. 16
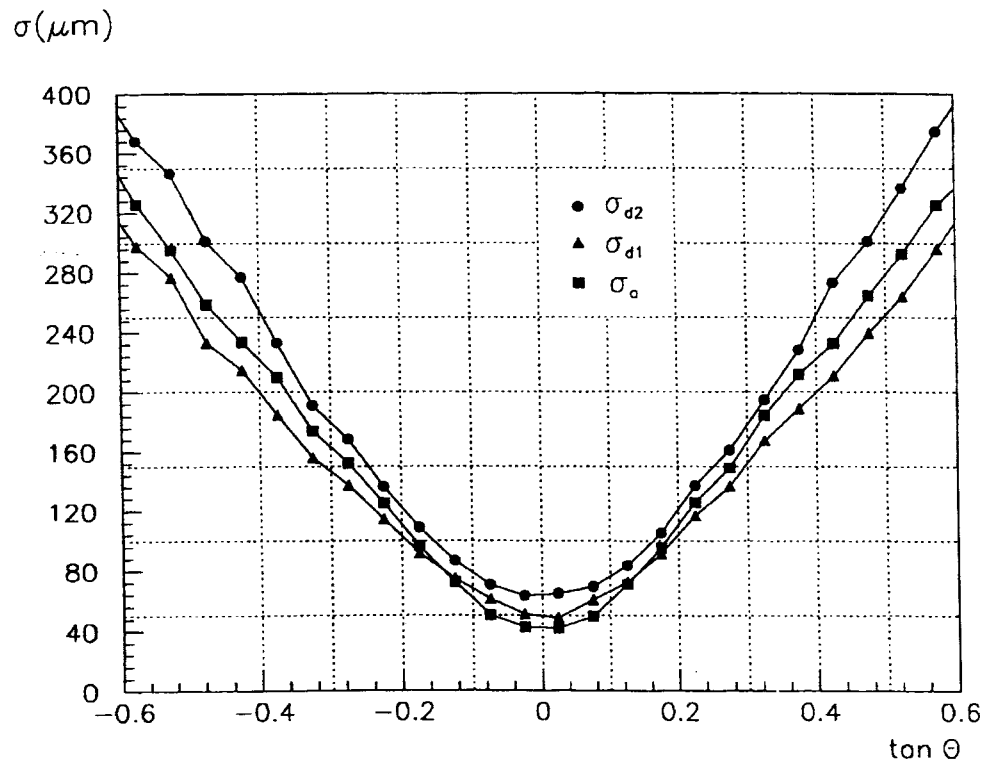
Fig. 17
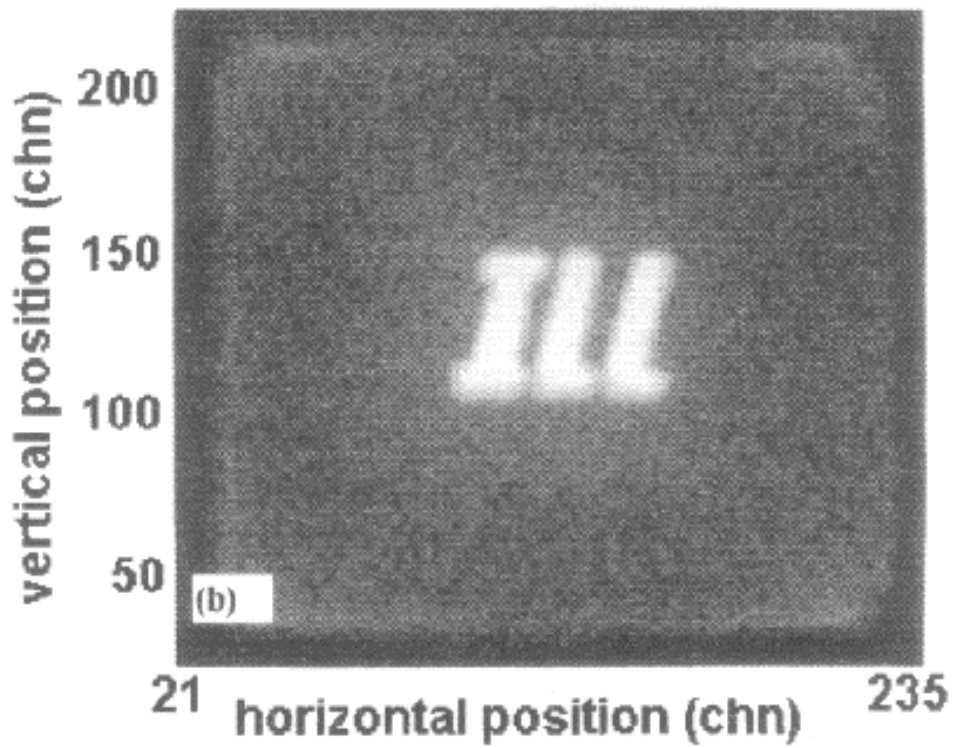
Fig. 18
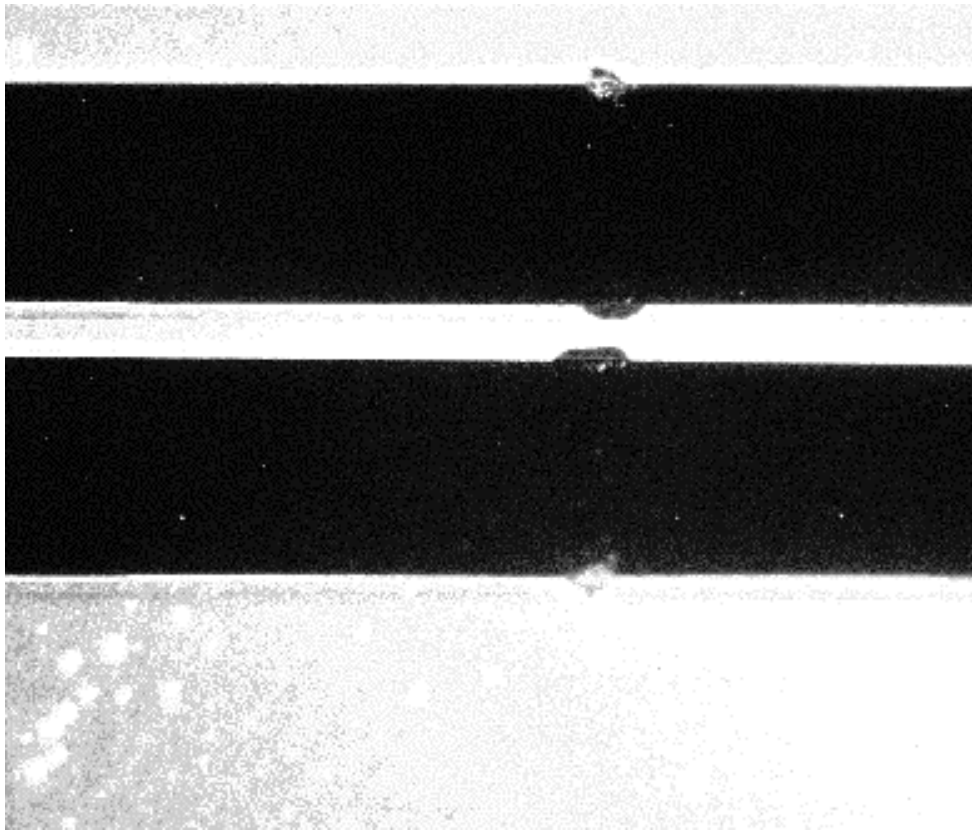
Fig. 19
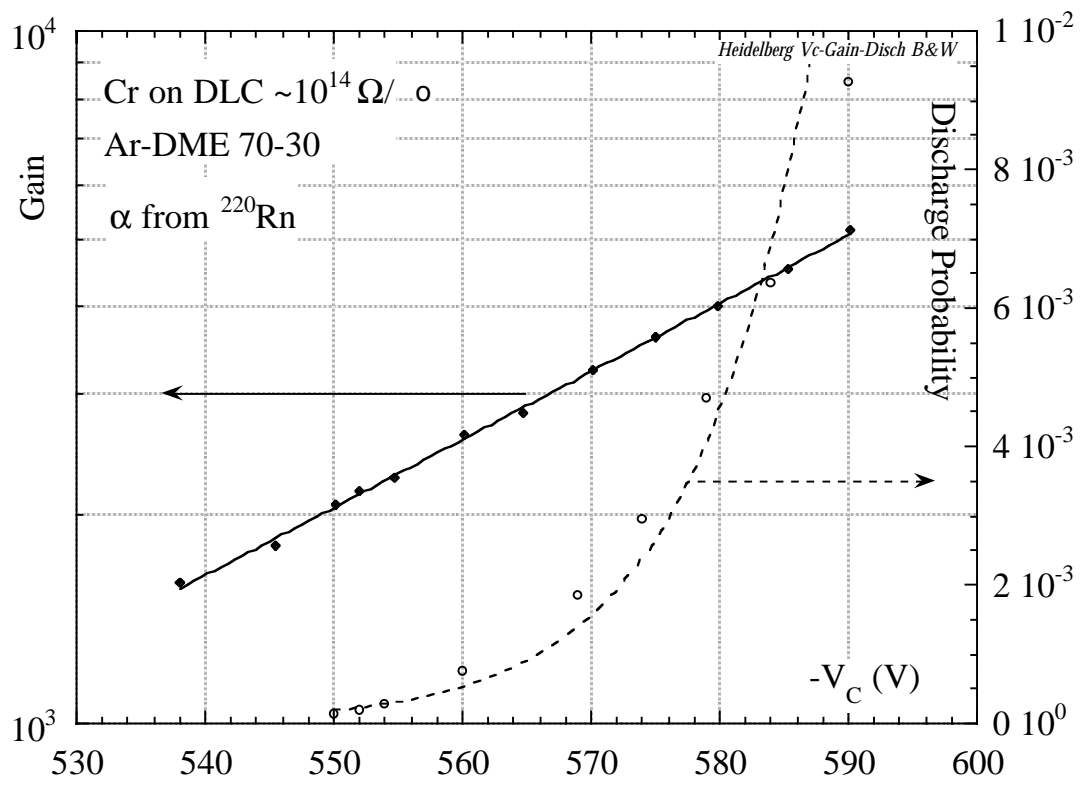
Fig. 20

Fig. 21

Fig. 22

Fig. 23

Fig. 24

ANODE CATHODE POLYIMIDE

ANODE CATHODE POLYIMIDE

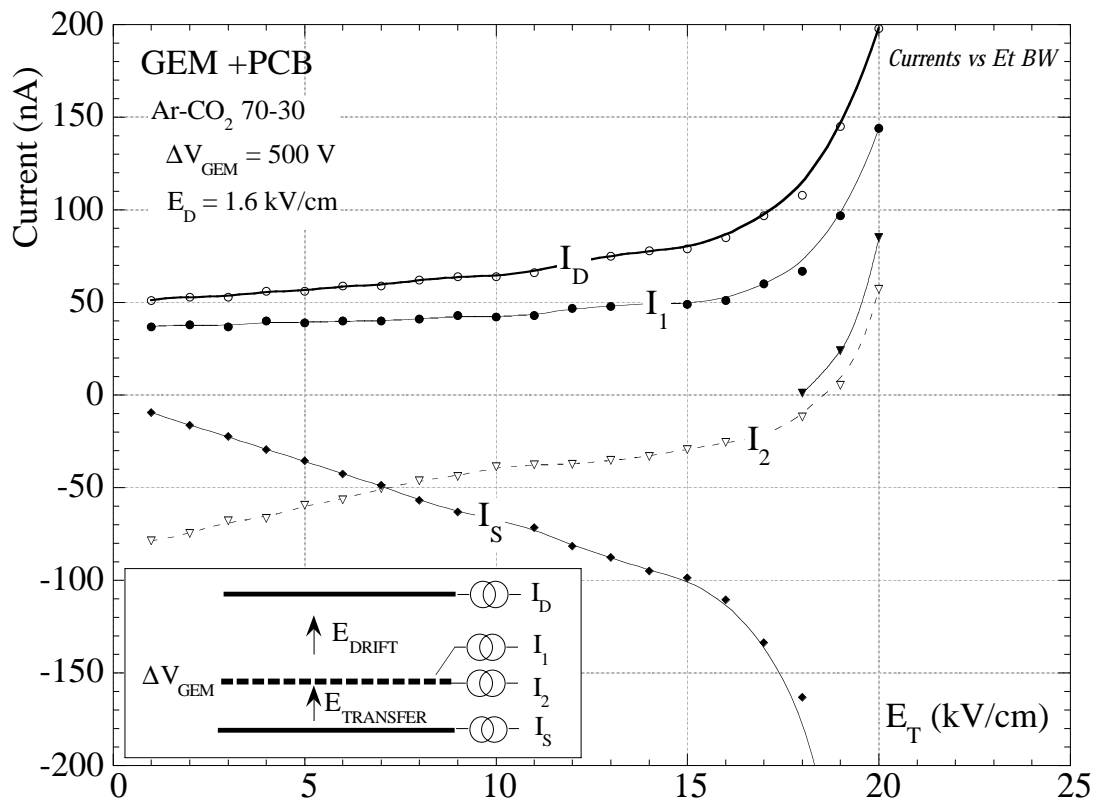Fig. 25

CATHODE ANODE DOT FIELD RING
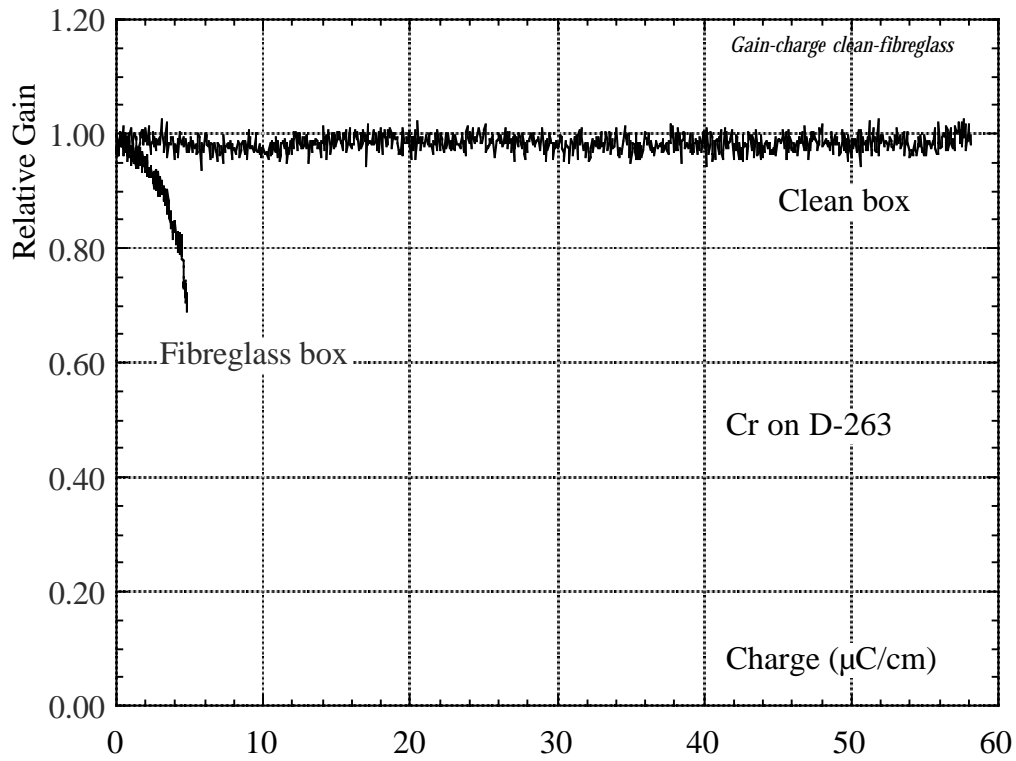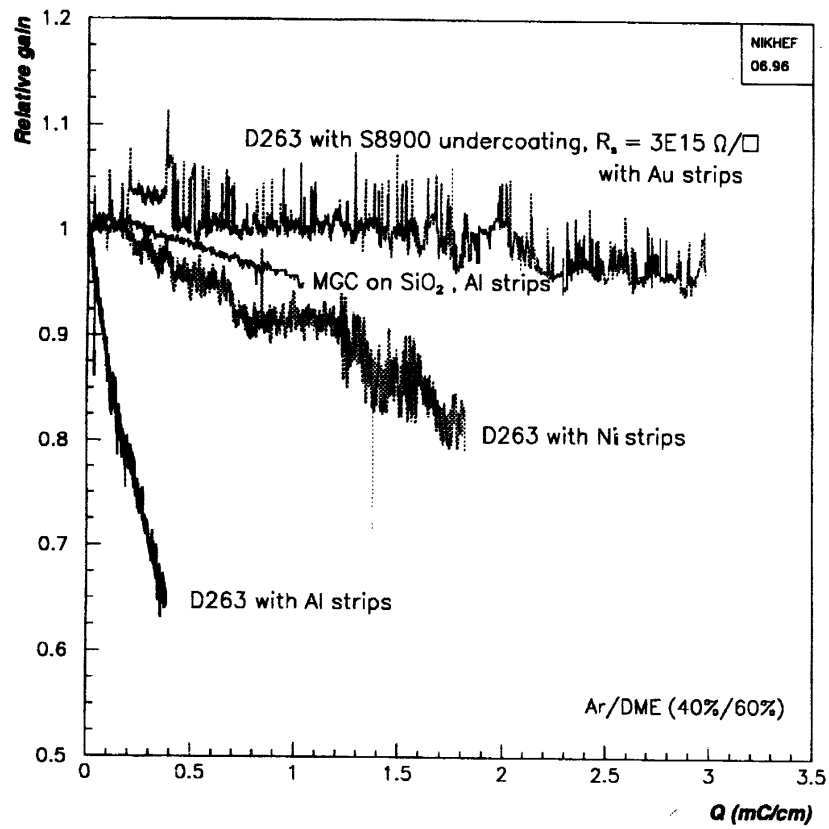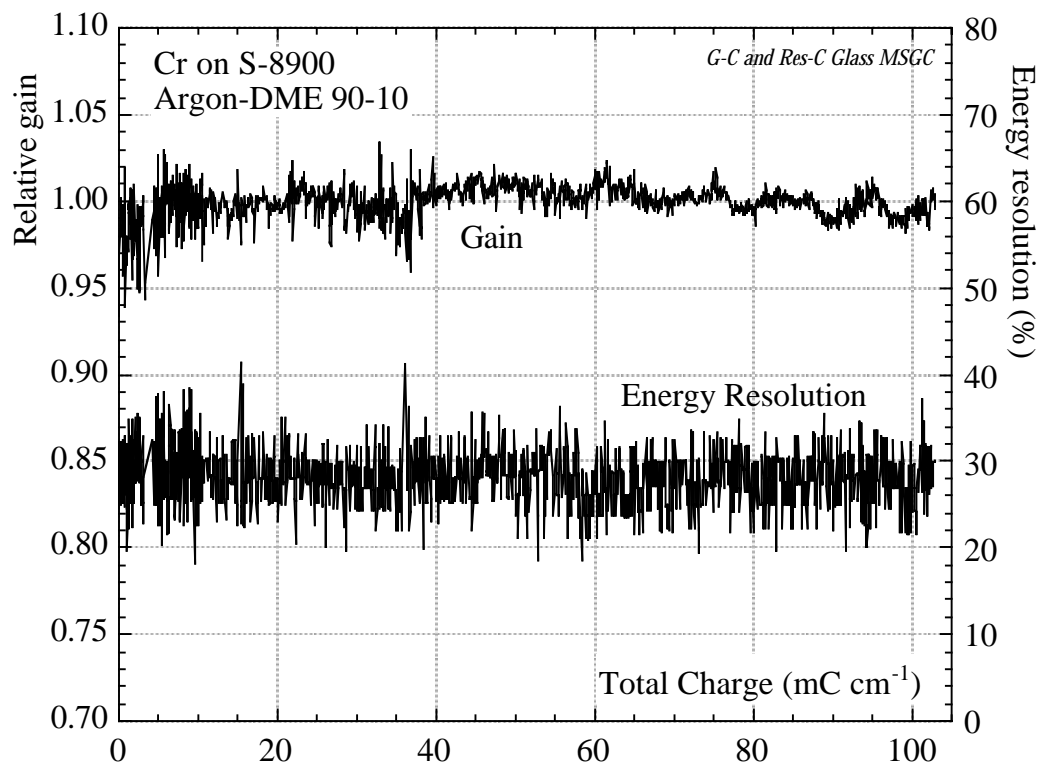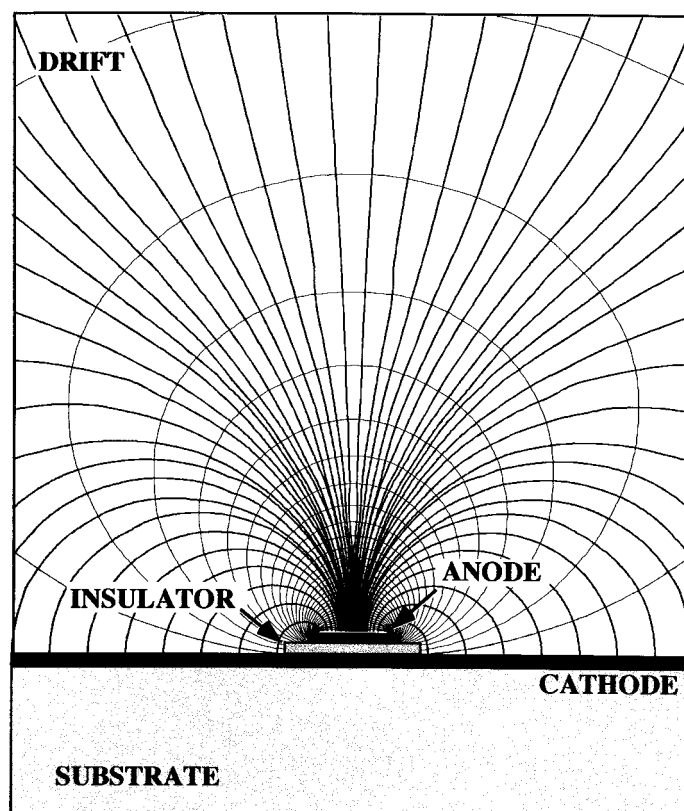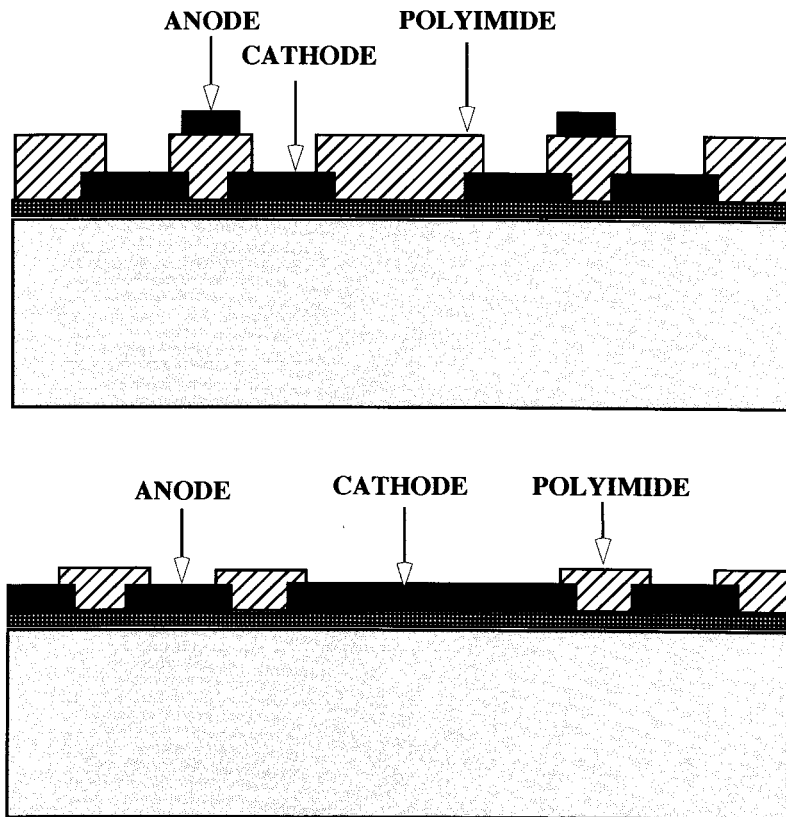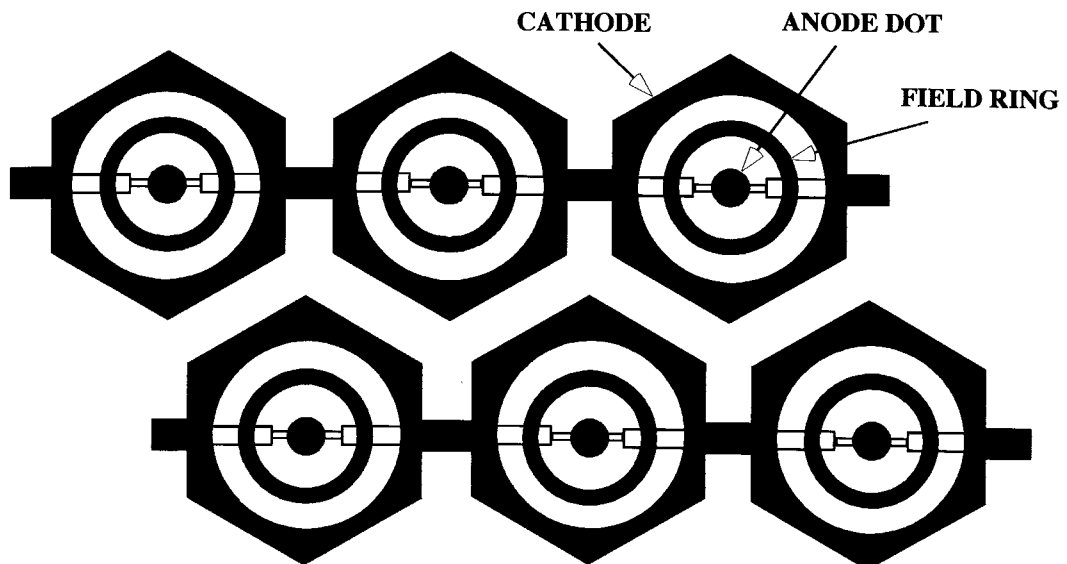
Fig. 26
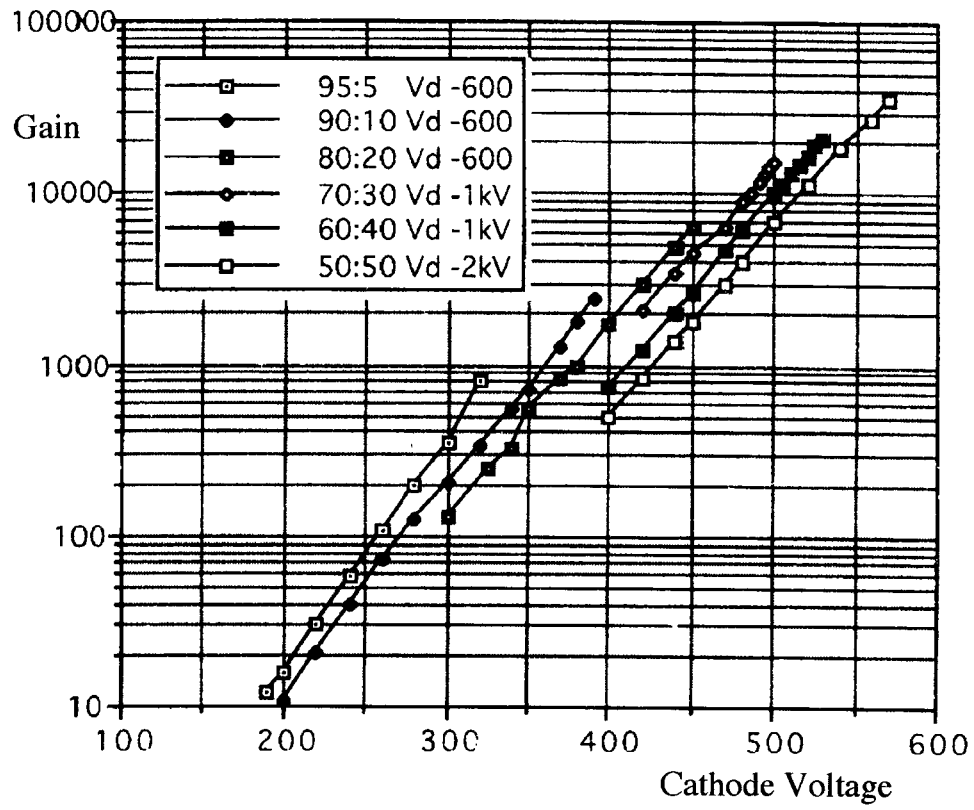
Fig. 27

Fig. 28

Fig. 29

Fig. 30

Fig. 31

Fig. 32

Fig. 33

Fig. 34

Fig. 35

Fig. 36

Fig. 37

Fig. 38

GEM +PCB

Ar-CO$_2$ 70-30

ΔV_{GEM} = 500 V

E_D = 1.6 kV/cm

Current (nA)

200

150

100

50

0

-50

-100

-150

-200

I_D

I_1

I_2

I_S

E_{DRIFT}

ΔV_{GEM}

$E_{TRANSFER}$

I_D

I_1

I_2

I_S

E_T (kV/cm)

0   5   10   15   20   25

Fig. 39

Double GEM + PCB

Argon-CO$_2$ 70-30

Efficiency (%)

Accuracy rms (μm)

100

90

80

70

60

50

100

80

60

40

20

0

Efficiency

Accuracy

$\Delta V_{GEM1} + \Delta V_{GEM2}$(V)

750   800   850   900   950   1000

Fig. 40

Fig. 41

Fig. 42